

HYDRA: Unifying Multi-modal Generation and Understanding via Representation-Harmonized Tokenization

Xuerui Qiu^{*123} Yutao Cui^{*2} Guozhen Zhang^{*4} Junzhe Li⁵ JiaKui Hu⁵ Xiao Zhang² Yang Li²
Songtao Liu² Miles Yang² Yu Shi³ Zhao Zhong² Liefeng Bo²

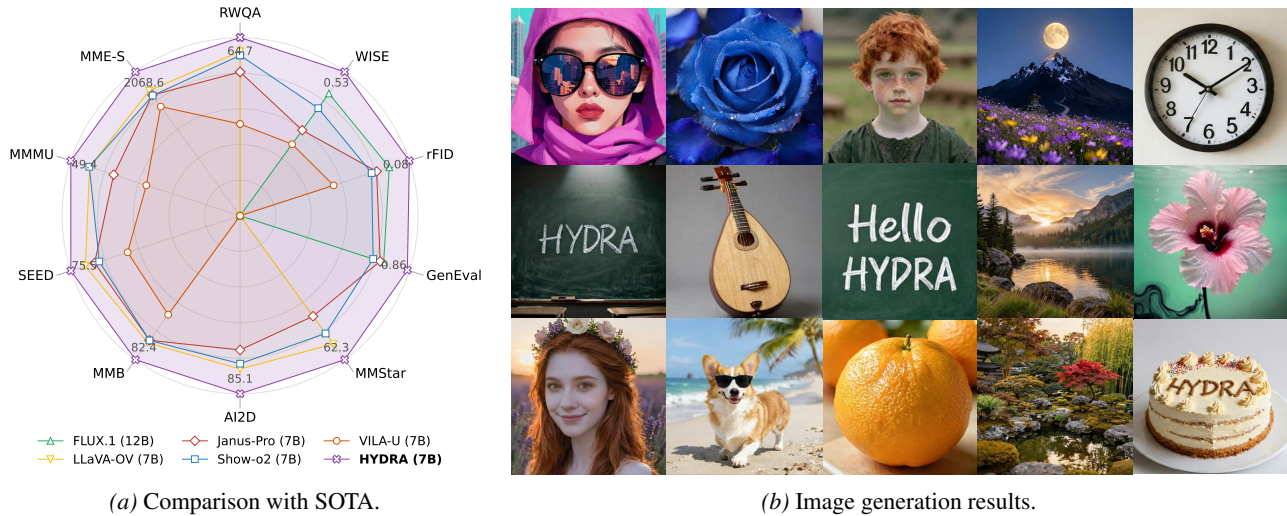


Figure 1. **Multimodal understanding and image generation results from HYDRA.** (a) Our model outperforms previous state-of-the-art unified multimodal models as well as several task-specific models across diverse benchmarks. (b) Our model demonstrates robust visual generation capabilities, producing high-fidelity images with accurate semantic alignment.

Abstract

Unified Multimodal Models struggle to bridge the fundamental gap between the abstract representations needed for visual understanding and the detailed primitives required for generation. Existing approaches typically compromise by employing decoupled encoders, stacking representation encoder atop VAEs, or utilizing discrete quantization. However, these methods often disrupt information coherence and lead to optimization conflicts. To this end, we introduce HYDRA-TOK, a representation-harmonized pure ViT in the insight that visual modeling should evolve from genera-

tion to understanding. HYDRA-TOK reformulates the standard backbone into a progressive learner that transitions from a Gen-ViT, which captures structure-preserving primitives, to a Sem-ViT for semantic encoding. Crucially, this transition is mediated by a Generation-Semantic Bottleneck (GSB), which compresses features into a low-dimensional space to filter noise for robust synthesis, then restores dimensionality to empower complex semantic comprehension. Built upon this foundation, we present HYDRA, a native unified framework integrating perception and generation within a single parameter space. Extensive experiments establish HYDRA as a new state-of-the-art. It sets a benchmark in visual reconstruction (rFID 0.08) and achieves top-tier generation performance on GenEval (0.86), DPG-Bench (86.4), and WISE (0.53), while simultaneously outperforming previous native UMMs by an average of ~ 10.0 points across eight challenging understanding benchmarks.

^{*}Equal contribution

^{*}We are actively scaling the model to larger parameter sizes. More updates coming soon. ¹Institute of Automation, Chinese Academy of Sciences ²Tencent Hunyuan ³Zhongguancun Academy ⁴Nanjing University ⁵Peking University. Correspondence to: Yu Shi <shiyu@bza.edu.cn>, Zhao Zhong <caesarqin@tencent.com>.

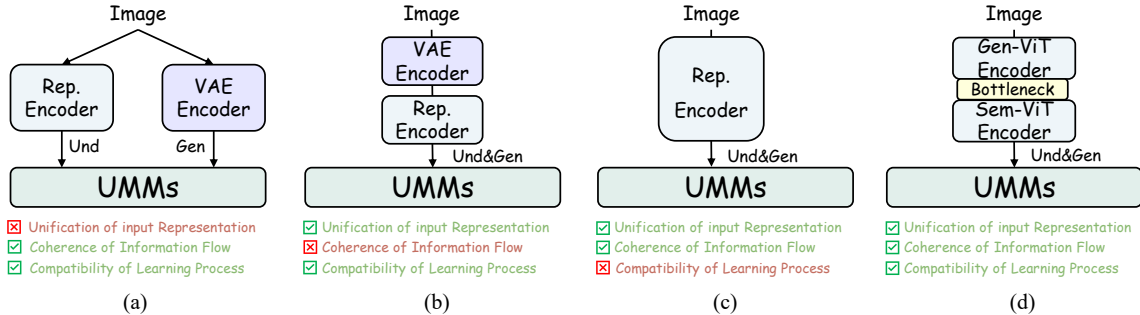


Figure 2. **Representation schemes in native unified multimodal models.** (a) Decoupled Encoder (Deng et al., 2025a; Wu et al., 2025a): It employs a VAE and a representation encoder as dedicated encoders for generation and understanding tasks, respectively. (b) Sequential Encoder (Xie et al., 2025a): It feeds the output of the VAE directly into the representation encoder in a cascaded manner. (c) Single-representation encoder (Ma et al., 2025a; Wu et al., 2025d): It adopts a standalone representation encoder to unify representation learning for both understanding and generation tasks. (d) Our Proposed Representation-Harmonized ViT Design: it also leverages a single ViT backbone, while introducing a bottleneck module to harmonize the feature learning processes of understanding and generation tasks.

1. Introduction

Unifying visual understanding and generation has emerged as a pivotal frontier in multimodal intelligence (Deng et al., 2025a; Cao et al., 2025; Liao et al., 2025b). Native unified multimodal models (UMMs) (Wu et al., 2025d; Zhou et al., 2024; Xie et al., 2025a) advocate for direct decoding within a unified parameter space, demonstrating superior synergy over composite UMMs (Ge et al., 2024; Tang et al., 2025; Chen et al., 2025a). However, achieving rational unification is hindered by a fundamental representational divergence, stemming from the fact that understanding and generation constitute inverse tasks with conflicting demands: the former necessitates high-level semantic abstractions, whereas the latter requires compact structural primitives for fine-grained synthesis (Radford et al., 2021; Kingma et al., 2019). This intrinsic conflict forces existing frameworks into disjointed, asymmetric designs, significantly increasing architectural complexity and optimization difficulty.

We attribute this dilemma primarily to the structural limitations of existing image tokenizers, which fail to simultaneously satisfy the three critical criteria illustrated in Fig. 2. First, decoupled paradigms that employ separate encoders for understanding and generation (Deng et al., 2025a; Cao et al., 2025) inherently lack *Unification of Input Representation*, relying on disjoint features that sever the synergy between the two tasks. Second, sequential architectures that stack representation encoders atop VAEs (Xie et al., 2025a; Liu et al., 2025) theoretically unify the input but compromise the *Coherence of Information Flow* due to the significant representation mismatch between the generative VAE latent space and the semantic features required by the representation encoder. Third, while utilizing a single shared representation encoder (Ma et al., 2025b; Wu et al., 2025d; Jiao et al., 2025) attempts to solve this, it often suffers from poor *Compatibility of Learning Process*, where the conflicting objectives of high-frequency detail

preservation and semantic abstraction lead to optimization difficulties. Consequently, current methods face an unavoidable trade-off: they either sacrifice generative fidelity, lose semantic alignment, or struggle to converge on a shared representation.

To address this, we propose HYDRA-TOK, a representation-harmonized pure ViT framework. Our core design principle is built on a key insight: a compact feature space capable of reconstructing input data can serve as a robust foundation for semantic understanding. This reconstruction task functions as an information bottleneck, compelling the compact feature to discard extraneous details and instead acquire a vocabulary of dense, structural primitives. These primitives provide a solid basis, thereby enabling the model to construct semantic abstractions from the ground up.

To this end, we reformulate a ViT-based representation encoder (Chen et al., 2024b;c) into a progressive learner that transitions from a Generation vision transformer (Gen-ViT), which captures structure-preserving primitives for high-fidelity synthesis, to a Semantic vision transformer (Sem-ViT). To unify these distinct objectives within a single model, we introduce the Generation-Semantic Bottleneck (GSB). The GSB is architected around a novel compress-and-reconstruct operation, creating an information bottleneck that fosters both high-level semantic abstraction and detailed generative fidelity. Specifically, GSB first compresses features into a compact low-dimension space to filter out noise component, then reconstructs them to the original space for subsequent semantic distillation. In this manner, the compact features can both encode structured details while maintaining semantic awareness.

Built upon HYDRA-TOK, we present HYDRA, a unified framework that achieves complete architectural and representational unification. Leveraging the coherent visual representations provided by HYDRA-TOK, visual

signals are processed as sequences via a dual-head mechanism, employing an autoregressive head for text prediction and a rectified flow matching head for image generation. Extensive experiments confirm that HYDRA achieves superior performance, highlighting the harmony between understanding and generation during joint training. In terms of multimodal understanding, HYDRA outperforms existing native UMMs by an average margin of approximately 10.0 points across eight benchmarks. Meanwhile, it establishes a new benchmark in visual reconstruction with a remarkable rFID of 0.08, providing a robust foundation that facilitates state-of-the-art generation records: 0.86 on GenEval (Ghosh et al., 2023), 86.4 on DPG-Bench (Hu et al., 2024), and 0.53 on WISE (Niu et al., 2025). Additionally, we find that joint training consistently outperforms separate training for both generation and understanding, validating the effectiveness of our harmonized representation. Our contributions are summarized as follows:

- We propose HYDRA-TOK, a representation-harmonized pure ViT that resolves the understanding-generation conflict via a progressive learner, unifying input representations without quantization errors.
- We present HYDRA, a native unified framework that integrates understanding and generation within a single parameter space, utilizing a dual-head mechanism for seamless task execution.
- Empirical results demonstrate that HYDRA outperforms native UMMs by ~ 10.0 points on understanding benchmarks and achieves state-of-the-art performance on GenEval, DPG-Bench, and WISE.

2. Method

We present HYDRA, a unified framework harmonizing visual understanding and generation. Central to our approach is HYDRA-TOK, a pure ViT grounded in a key insight: a compact feature space capable of reconstructing inputs serves as a robust foundation for semantic understanding. Adopting a functionally progressive learner design (Fig. 3), we transition continuously from structure-preserving primitives (Gen-ViT) to semantic abstractions (Sem-ViT). This is realized via the Generation-Semantic Bottleneck (GSB) and its novel compress-and-reconstruct operation. By compressing features to filter noise and reconstructing them for distillation, the GSB effectively balances generative fidelity with semantic awareness.

2.1. HYDRA-TOK

Traditional tokenizers face a rigid trade-off between preserving semantic depth and maintaining structural detail. To

resolve this issue, HYDRA-TOK reformulates the complete vision transformer backbone into three functionally distinct yet continuous components, effectively followed by a lightweight flow-based decoder.

Generation Vision Transformer (Gen-ViT). Given an input image $\mathbf{x} \in \mathbb{R}^{H \times W \times 3}$, we first flatten and project non-overlapping patches into continuous embeddings $\mathbf{H}_0 \in \mathbb{R}^{N \times D}$, where N and D correspond to the number of tokens and dimension. The initial stage, Gen-ViT, is tasked with extracting low-level structural primitives essential for generation. Unlike standard encoders that aggressively compress spatial information, Gen-ViT preserves fine-grained spatial covariance:

$$\mathbf{H}_{\text{mid}} = \text{Gen-ViT}(\mathbf{H}_0) = \Phi_{L_{\text{gen}}} \circ \dots \circ \Phi_1(\mathbf{H}_0), \quad (1)$$

where Φ_l denotes the l -th transformer block. This phase ensures that the latent space retains the structural foundation required for high-fidelity synthesis.

Generation-Semantic Bottleneck (GSB). To transition from structure-preserving primitives to semantic abstractions, we introduce the GSB block. Built on a compress-and-reconstruct operation, GSB serves as an information bottleneck that filters extraneous noise to balance the conflicting demands of understanding and generation. As evidenced by our ablation (Fig. 4), while higher dimensions (C) aid reconstruction and understanding, they cause generation performance to collapse (e.g., at $C \geq 256$). This confirms that excessive dimensionality introduces redundancy that disrupts generative stability.

To resolve this, GSB acts as a stabilization pivot by first compressing the intermediate features \mathbf{H}_{mid} into a compact probabilistic space via a lightweight projector $\mathbf{W}_{\text{proj}} \in \mathbb{R}^{D \times C}$, where $C \ll D$ (typically 64):

$$[\boldsymbol{\mu}, \boldsymbol{\rho}] = \mathbf{W}_{\text{proj}} \mathbf{H}_{\text{mid}}, \quad \mathbf{z} = \boldsymbol{\mu} + \boldsymbol{\epsilon} \odot \exp(0.5\boldsymbol{\rho}), \quad (2)$$

where $\boldsymbol{\mu}, \boldsymbol{\rho} \in \mathbb{R}^{N \times C}$ represent the mean and log-variance, and $\boldsymbol{\epsilon} \sim \mathcal{N}(\mathbf{0}, \mathbf{I})$ is reparameterization noise.

To structure this latent space, we impose a KL divergence loss that aligns the posterior with a standard normal prior:

$$\mathcal{L}_{\text{KL}} = -\frac{1}{2} \sum_{j=1}^C (1 + \rho_j - \mu_j^2 - \exp(\rho_j)). \quad (3)$$

To maintain a coherent flow of information under compression and provide a sufficient foundation for subsequent semantic extraction, we introduce a consistency loss \mathcal{L}_{cos} . This loss forces the unprojected features $\mathbf{H}_{\text{bn}} = \boldsymbol{\mu} \mathbf{W}_{\text{unproj}}^{\text{und}}$ to maintain directional alignment with the pre-bottleneck features \mathbf{H}_{mid} :

$$\mathcal{L}_{\text{cos}} = 1 - \frac{\mathbf{H}_{\text{mid}} \cdot \mathbf{H}_{\text{bn}}}{\|\mathbf{H}_{\text{mid}}\|_2 \|\mathbf{H}_{\text{bn}}\|_2}. \quad (4)$$

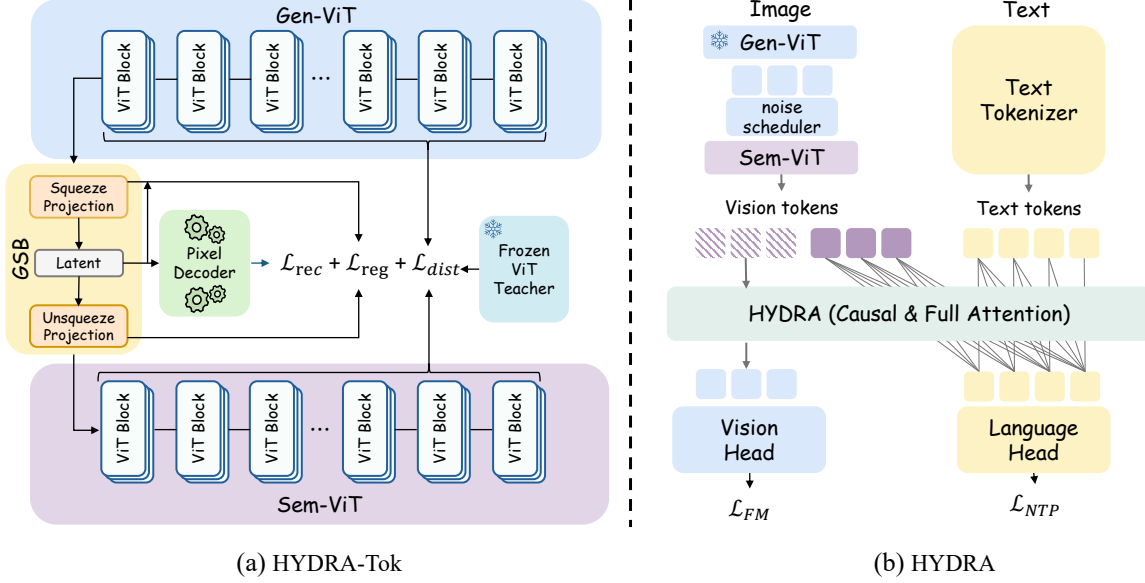


Figure 3. **Training process illustration for HYDRA-TOK and HYDRA.** (a) HYDRA-TOK functions as a progressive learner, bridging the gap between reconstruction and understanding. It employs a Generation-Semantic Bottleneck (GSB) to execute a unique compress-and-reconstruct operation, effectively filtering noise to transition from structure-preserving primitives (Gen-ViT) to semantic abstractions (Sem-ViT). (b) HYDRA achieves representational unification upon this foundation, utilizing a dual-head mechanism to seamlessly integrate autoregressive text prediction with rectified flow matching for image generation.

Based on our experiments, we set the regularization weights to $\lambda_{KL} = 10^{-4}$ and $\lambda_{cos} = 1.0$. The composite bottleneck objective is defined as $\mathcal{L}_{reg} = \lambda_{KL}\mathcal{L}_{KL} + \lambda_{cos}\mathcal{L}_{cos}$.

Semantic Vision Transformer (Sem-ViT). As the final stage of our functionally progressive learner, Sem-ViT acts as a deep non-linear mapper. Its primary role is to transition the structural foundations (encoded in \mathbf{H}_{bn}) into a high-dimensional semantic space, thereby achieving rational disentanglement:

$$\mathbf{H}_{out} = \text{Sem-ViT}(\mathbf{H}_{bn}) = \Phi_{L_{total}} \circ \dots \circ \Phi_{L_{gen+1}}(\mathbf{H}_{bn}). \quad (5)$$

To ensure robust representation learning across the entire hierarchy, we employ semantic self-distillation on both Gen-ViT and Sem-ViT. We align the intermediate features from distinct depths of the student with a frozen, pre-trained ViT (Chen et al., 2024b) via cosine similarity maximization:

$$\mathcal{L}_{dist} = \sum_{l \in \mathcal{S}_{gen} \cup \mathcal{S}_{sem}} \left(1 - \frac{\mathbf{H}^{(l)}(\mathbf{x}) \cdot \mathcal{T}^{(l)}(\mathbf{x})}{\|\mathbf{H}^{(l)}(\mathbf{x})\|_2 \|\mathcal{T}^{(l)}(\mathbf{x})\|_2} \right), \quad (6)$$

where \mathcal{S}_{gen} and \mathcal{S}_{sem} denote the selected layers from Gen-ViT and Sem-ViT, respectively.

Pixel Flow Decoder. To unburden the backbone, we employ a lightweight decoder \mathbf{v}_θ that utilizes flow matching to recover high-frequency details. Conditioned on latent \mathbf{c} , it learns to regress the velocity field by minimizing:

$$\mathcal{L}_{FM} = \mathbb{E}_{t, \mathbf{x}, \epsilon} [\|\mathbf{v}_\theta(\mathbf{x}_t, t, \mathbf{c}) - (\epsilon - \mathbf{x})\|^2]. \quad (7)$$

To further enhance perceptual fidelity, we enforce an LPIPS loss \mathcal{L}_{lpiips} on the estimated clean image $\hat{\mathbf{x}}$ and incorporate an adversarial GAN loss \mathcal{L}_{gan} to refine texture realism. We empirically set $\lambda_{FM} = 1.0$, $\lambda_{perc} = 0.1$, and $\lambda_{gan} = 0.075$. The total reconstruction loss is formulated as $\mathcal{L}_{rec} = \lambda_{FM}\mathcal{L}_{FM} + \lambda_{perc}\mathcal{L}_{lpiips} + \lambda_{gan}\mathcal{L}_{gan}$.

Total objective. Finally, the unified tokenizer is optimized by minimizing the weighted sum of the reconstruction, regularization, and alignment objectives defined above:

$$\mathcal{L}_{tokenizer} = \mathcal{L}_{rec} + \mathcal{L}_{reg} + \lambda_{dist}\mathcal{L}_{dist}, \quad (8)$$

where the distillation weight is set to $\lambda_{dist} = 1.0$ by default.

2.2. HYDRA

Built upon the robust representations of HYDRA-TOK, HYDRA represents a native unified framework that integrates understanding and generation within a single parameter space. By leveraging the coherent visual representations from our tokenizer, HYDRA processes visual and textual signals as a unified sequence via a shared autoregressive transformer, employing a specialized dual-head mechanism to reconcile their distinct output modalities.

Unified Input Representation. To achieve the *Unification of Input Representation*, we integrate visual signals into the LLM by treating them as continuous sequences fully compatible with the embedding space. For a given image, we extract its latent representation \mathbf{H}_{bn} from the GSB. We

implement a task-aware injection strategy: for flow-based generation, we introduce diffusion noise corresponding to the time-step t ($\mathbf{H}_{in} = \mathbf{H}_{bn} + t\epsilon$); conversely, for understanding, we utilize the clean, deterministic latents to maximize semantic clarity. These processed latents are mapped to the LLM’s dimension via a linear projector to yield \mathbf{U}_{vis} . Finally, we concatenate them with text embeddings \mathbf{E}_{text} to form a unified input stream:

$$\mathbf{U}_{in} = [\mathbf{E}_{text}, \mathbf{U}_{vis}]. \quad (9)$$

Dual-Head Decoding. The unified sequence \mathbf{U}_{in} is processed by the shared LLM backbone. Following standard UMM practices (Xie et al., 2025a; Deng et al., 2025a), we apply a causal attention mask on language tokens and a bidirectional attention mask on visual tokens within the LLM decoder layers. To address the *Compatibility of Learning Process* between discrete text prediction and continuous image synthesis, we branch the output of the final transformer layer into two specialized heads. The Language Head (autoregressive) functions as a standard linear classifier, predicting the probability distribution over the text vocabulary based on the unified context: $\mathcal{L}_{NTP} = -\sum \log P(y_i | y_{<i}, \mathbf{U}_{in})$. Simultaneously, the Vision Head (diffusion) serves as a continuous regression head modulated by time-step embeddings via AdaLN-Zero (Peebles & Xie, 2023). This head operates explicitly on the hidden states corresponding to visual tokens (\mathbf{H}_{LLM}^{vis}) to predict the flow velocity:

$$\mathbf{v}_{pred} = \text{Head}_{flow}(\text{AdaLN}(\mathbf{H}_{LLM}^{vis}, t_{emb})). \quad (10)$$

Unified Training Objective. HYDRA is trained end-to-end via a composite objective:

$$\mathcal{L}_{total} = \mathcal{L}_{NTP} + \mathcal{L}_{FM}. \quad (11)$$

By sharing the LLM backbone while specializing only the input and output layers, HYDRA achieves rational unification.

2.3. Training Recipe

To cultivate the harmonized nature of HYDRA, we implement a three-stage progressive training strategy. We initialize HYDRA-TOK via reconstruction on large-scale corpora combined with semantic self-distillation against a teacher ViT (Chen et al., 2024b). Subsequent stages incrementally refine the compatibility between understanding and generation (see Appendix D for full data details).

Stage I: Unified Representation Alignment. To resolve the representation divergence at the input level, we freeze the LLM and exclusively tune the vision components. Utilizing 100M image-text pairs, this phase aligns the visual latent space with the linguistic domain, ensuring a coherent unified input representation.

Table 1. Reconstruction quality on the ImageNet-1K (256 × 256) and MS-COCO 2017 validation sets. , following the evaluation protocol in (Yue et al., 2025). \dagger indicates that the model is trained strictly on the ImageNet-1.2M dataset (Russakovsky et al., 2014)

| Method | ImageNet-1K | | | MS-COCO 2017 | | |
|--|-----------------|-----------------|-------------------|-----------------|-----------------|-------------------|
| | PSNR \uparrow | SSIM \uparrow | rFID \downarrow | PSNR \uparrow | SSIM \uparrow | rFID \downarrow |
| <i>Generative Only Tokenizer</i> | | | | | | |
| SD-VAE (Rombach et al., 2022) | 23.54 | 0.68 | 1.22 | 26.62 | 0.77 | 4.26 |
| SD-VAE XL (Podell et al., 2023) | 27.37 | 0.78 | 0.67 | 27.08 | 0.80 | 3.93 |
| SD-VAE 3 (Esser et al., 2024) | 31.29 | 0.87 | 0.20 | 31.18 | 0.89 | 1.67 |
| FLUX-VAE (Labs et al., 2025) | 32.74 | 0.92 | 0.18 | 32.32 | 0.93 | 1.35 |
| VA-VAE \dagger (Yao et al., 2025b) | 27.96 | 0.79 | 0.28 | 27.50 | 0.81 | 2.71 |
| Wan2.2 (Wan et al., 2025) | 31.25 | 0.88 | 0.75 | 31.10 | 0.89 | 3.28 |
| FlowMo-Hi \dagger (Shaulov et al., 2025) | 26.93 | 0.79 | 0.56 | – | – | – |
| <i>Unified Tokenizer</i> | | | | | | |
| Tokenflow (Qu et al., 2025) | 21.41 | 0.69 | 1.37 | – | – | – |
| UniTok (Ma et al., 2025b) | 27.28 | 0.77 | 0.41 | – | – | – |
| UniLIP (Tang et al., 2025) | 22.99 | 0.747 | 0.79 | – | – | – |
| EMU2 (Sun et al., 2024) | 13.49 | 0.42 | 3.27 | – | – | – |
| BLIP3-o (Chen et al., 2025a) | 14.71 | 0.58 | 3.18 | – | – | – |
| QLIP (Zhao et al., 2025) | 23.16 | 0.63 | 3.21 | – | – | – |
| UAE \dagger (Fan et al., 2025) | 29.65 | 0.88 | 0.19 | 29.47 | 0.88 | 2.04 |
| UniFlow \dagger (Yue et al., 2025) | 33.23 | 0.96 | 0.26 | 32.48 | 0.95 | 1.88 |
| RAE \dagger (Zheng et al., 2025) | 18.05 | 0.50 | 2.04 | – | – | – |
| HYDRA-TOK\dagger | 37.09 | 0.97 | 0.12 | 35.63 | 0.98 | 1.05 |
| HYDRA-TOK | 36.39 | 0.96 | 0.08 | 35.94 | 0.96 | 0.81 |

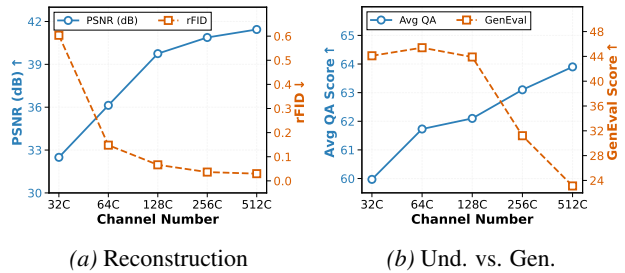


Figure 4. Ablation results on different latent channel dimensions.

Stage II: Comprehensive Multimodal Pre-training. We unlock all parameters to facilitate harmonized co-promotion within a single unified stream. The model is jointly optimized on a balanced mix of 30M understanding samples and 30M generative samples (strategically filtered from Stage I). This full-parameter update ensures the *Compatibility of Learning Process*, allowing the two tasks to mutually reinforce each other.

Stage III: High-Quality Instruction Fine-tuning. The final stage focuses on high-fidelity refinement using curated datasets. We employ 3.2M balanced instruction-tuning samples for understanding, alongside 10M aesthetic-filtered images (derived from Stage II) and 6M high-fidelity synthetic images for generation.

3. Experiments

We conduct extensive experiments to evaluate how HYDRA addresses the fundamental challenges in unified multimodal learning identified in the Introduction:

- **RQ1:** What is the sweet spot between high-level se-

Table 2. Evaluation on multimodal understanding benchmarks. # Params. and # Data denote the model size and the volume of image-text pairs used for instruction tuning, respectively. MME-S represents the aggregate of MME-P and MME-C. Avg. reports the average normalized score across all benchmarks (where MME-S is normalized by 2,800). Rows in gray indicate models exceeding 14B parameters.

| Models | # Params | # Data | MME-S | A12D | OCRBench | MMB | RWQA | SEED | MMMU | MMStar | Avg. |
|---|----------|--------|---------------|-------------|-------------|-------------|-------------|-------------|-------------|-------------|-------------|
| <i>Understanding-only Models</i> | | | | | | | | | | | |
| Qwen2.5-VL (Bai et al., 2023) | 3B | 1B+ | 2199.9 | 81.4 | 82.8 | 77.6 | 65.5 | 74.0 | 51.2 | 56.3 | 70.9 |
| Qwen2.5-VL (Bai et al., 2023) | 7B | 1B+ | 2312.0 | 84.3 | 88.8 | 82.8 | 68.4 | 77.0 | 58.0 | 64.1 | 75.7 |
| LLaVA-1.5 (Liu et al., 2023b) | 7B | 0.7M | 1510.7 | 55.5 | 31.8 | 62.3 | 54.8 | 65.8 | 35.7 | 33.1 | 49.1 |
| LLaVA-OV (Li et al., 2024b) | 7B | 3.2M | 1998.1 | 81.4 | 62.2 | 80.8 | 66.3 | 76.7 | 48.8 | 61.7 | 68.7 |
| <i>Composite Unified Multimodal Models</i> | | | | | | | | | | | |
| BLIP3-o (Chen et al., 2025a) | 4B | N/A | 2161.2 | - | - | - | 60.4 | 73.8 | 46.6 | - | - |
| TokenFlow-XL (Qu et al., 2025) | 14B | N/A | 1922.1 | - | - | 68.9 | 56.6 | 72.6 | 43.2 | - | - |
| SEED-X (Ge et al., 2024) | 17B | N/A | 1457.0 | 70.0 | - | 70.1 | 49.1 | 65.6 | 35.6 | - | - |
| <i>Smaller Native Unified Multimodal Models</i> | | | | | | | | | | | |
| Show-o (Xie et al., 2024) | 1.3B | 0.7M | 1345.1 | - | - | - | - | 51.5 | 27.4 | - | - |
| JanusFlow (Ma et al., 2025c) | 1.3B | 1.4M | 1560.1 | 54.2 | - | 69.4 | 41.2 | 70.5 | 29.3 | 40.6 | - |
| Janus-Pro (Chen et al., 2025b) | 1.5B | 10M | 1875.1 | 64.5 | - | 75.5 | 52.6 | 68.3 | 36.3 | 43.1 | - |
| Harmon (Wu et al., 2025d) | 1.5B | 3.2M | 1476.2 | 57.0 | 11.2 | 67.1 | 49.8 | 67.1 | 38.9 | 35.3 | 47.4 |
| Show-o2 (Xie et al., 2025a) | 1.5B | 3.2M | 1742.3 | 69.0 | 24.5 | 67.4 | 56.5 | 65.6 | 37.1 | 43.4 | 53.2 |
| HYDRA | 1.5B | 3.2M | 1877.9 | 79.4 | 50.8 | 76.8 | 60.7 | 74.5 | 39.1 | 57.0 | 63.2 |
| <i>Larger Native Unified Multimodal Models</i> | | | | | | | | | | | |
| Ming-UniVision (Huang et al., 2025) | 16B | 20M+ | 2023.0 | 82.8 | 72.4 | 78.5 | - | - | 40.3 | 63.7 | - |
| BAGEL (Deng et al., 2025b) | 14B | 15.2M | 2388.0 | 89.2 | 73.3 | 85.0 | 72.8 | 78.5 | 55.3 | - | - |
| MUSE-VL (Xie et al., 2025b) | 7B | 10M | - | 69.8 | - | 72.1 | - | 69.1 | 39.7 | 49.6 | - |
| Janus-Pro (Chen et al., 2025b) | 7B | 10M | 1927.1 | 71.3 | - | 79.2 | 58.0 | 72.1 | 41.0 | 48.3 | - |
| VILA-U (Wu et al., 2024) | 7B | 4M | 1845.8 | - | - | 66.6 | - | 59.0 | 32.2 | - | - |
| Show-o2 (Xie et al., 2025a) | 7B | 3.2M | 1920.5 | 78.6 | 32.4 | 79.3 | 64.7 | 69.8 | 48.9 | 56.6 | 62.4 |
| HYDRA | 7B | 3.2M | 2068.6 | 85.1 | 57.7 | 82.4 | 64.7 | 75.5 | 49.4 | 62.3 | 68.9 |

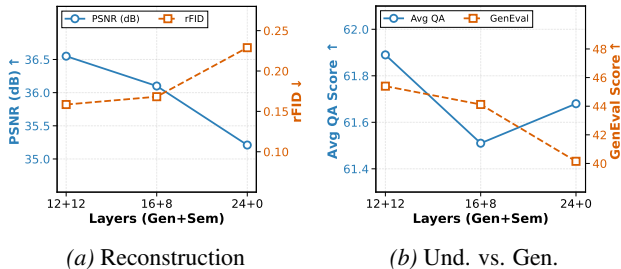


Figure 5. Ablation results on different layer configurations.

mantic abstraction and compact structural synthesis in HYDRA-TOK to achieve a rational unified representation?

- **RQ2:** Can a pure ViT-based tokenizer HYDRA-TOK achieve state-of-the-art reconstruction fidelity?
- **RQ3:** Does the pure ViT architecture HYDRA preserve the coherence of information flow better than VAE-based or decoupled approaches, thereby enhancing multimodal understanding?
- **RQ4:** Does the joint optimization of autoregressive and flow-matching objectives achieve compatibility, enabling state-of-the-art generative performance?

Implementation Details. We evaluate HYDRA at two scales: 1.5B (based on Qwen2.5-1.5B-Instruct (Yang et al.,

2024)) and 7B (Qwen2.5-7B-Instruct). The HYDRA-TOK is initialized with InternViT-2.5 (Chen et al., 2024b) to leverage robust visual priors. The training recipe employs a three-stage progressive pipeline optimized with AdamW (Loshchilov & Hutter, 2017). The specific learning rate schedules for each stage are detailed in Tab. 6. For comprehensive experimental details and evaluation metrics regarding all ablation studies, please refer to Appendix D.1.

3.1. Main Results

RQ1: Identifying the Sweet Spot for Rational Unification. Achieving a rational unified representation requires identifying the optimal synergy between high-level semantic abstraction and compact structural synthesis within a single feature space. We seek the architectural “sweet spot” where both capabilities are maximized simultaneously, rather than viewing them as competing objectives. As initially determined regarding channel dimensions (referencing Fig. 4), incorporating the GSB to compress the feature space to $C = 64$ represents the representational sweet spot, achieving *Unification of Input Representation* by filtering redundant noise while retaining semantic capacity. Further investigating this balance at the architectural level, Fig. 5 illustrates the impact of different layer allocations. We observe that configurations deviating from a balanced structure fail to achieve optimal synergy. The highly imbalanced 24 + 0 configuration (pure Gen-ViT) exhibits the poorest performance

Table 3. Comprehensive image generation results on GenEval (Ghosh et al., 2023), DPG-Bench (Hu et al., 2024), and WISE (Niu et al., 2025). # Data. indicates the number of image-text pairs used for visual generation. † refers to finetuning with GPT-4o distilled synthetic dataset (Chen et al., 2025a). More Visualization can be founded in Appendix G.2.

| Models | # Params | # Data | GenEval | | | DPG-Bench | | | WISE | | |
|---|----------|--------|-------------|-------------|-------------|--------------|--------------|--------------|-------------|-------------|-------------|
| | | | Two Obj. | Pos. | Over. | Glob. | Rel. | Over. | Cult. | Space | Over. |
| <i>Generation-only Models</i> | | | | | | | | | | | |
| SD3-Med (Esser et al., 2024) | 2B | 1B+ | 0.94 | 0.33 | 0.74 | - | - | 84.08 | - | - | - |
| FLUX.1 [Dev] (Labs et al., 2025) | 12B | 1B+ | 0.93 | 0.68 | 0.82 | 82.10 | 91.10 | 84.00 | 0.48 | 0.62 | 0.50 |
| <i>Composite Unified Multimodal Models</i> | | | | | | | | | | | |
| Blip3-o† (Chen et al., 2025a) | 4B | 30M | - | - | 0.84 | - | - | 79.36 | - | - | 0.50 |
| TokenFlow-XL (Qu et al., 2025) | 14B | 60M | 0.60 | 0.16 | 0.55 | 87.53 | 90.30 | 85.02 | - | - | - |
| SEED-X (Ge et al., 2024) | 17B | 158M+ | 0.58 | 0.19 | 0.49 | - | - | - | - | - | - |
| <i>Smaller Native Unified Multimodal Models</i> | | | | | | | | | | | |
| Show-o (Xie et al., 2024) | 1.3B | 36M | 0.52 | 0.11 | 0.53 | - | - | 67.27 | - | - | 0.35 |
| Harmon (Wu et al., 2025d) | 1.5B | 100M | 0.86 | 0.74 | 0.76 | - | - | - | 0.38 | 0.52 | 0.41 |
| Show-o2 (Xie et al., 2025a) | 1.5B | 66M | 0.86 | 0.46 | 0.73 | 87.53 | 90.30 | 85.02 | 0.33 | 0.53 | 0.39 |
| HYDRA | 1.5B | 100M | 0.95 | 0.76 | 0.86 | 89.65 | 91.59 | 85.51 | 0.49 | 0.64 | 0.49 |
| <i>Larger Native Unified Multimodal Models</i> | | | | | | | | | | | |
| Ming-UniVision (Huang et al., 2025) | 16B | 1B+ | 0.93 | 0.92 | 0.85 | - | - | 82.12 | - | - | - |
| BAGEL (Deng et al., 2025b) | 14B | 1.6B | 0.95 | 0.78 | 0.88 | 88.94 | 90.82 | 85.07 | 0.44 | 0.68 | 0.52 |
| MUSE-VL (Xie et al., 2025b) | 7B | 24M | 0.64 | 0.25 | 0.57 | - | - | - | - | - | - |
| Janus-Pro (Chen et al., 2025b) | 7B | 144M | 0.89 | 0.79 | 0.80 | 86.90 | 89.32 | 84.19 | 0.30 | 0.49 | 0.35 |
| VILA-U (Wu et al., 2024) | 7B | 15M | - | - | - | - | - | - | 0.26 | 0.37 | 0.31 |
| Show-o2 (Xie et al., 2025a) | 7B | 66M | 0.87 | 0.52 | 0.76 | 89.00 | 91.81 | 86.14 | 0.40 | 0.58 | 0.44 |
| HYDRA | 7B | 100M | 0.97 | 0.81 | 0.86 | 90.22 | 91.83 | 86.40 | 0.52 | 0.68 | 0.53 |

Table 4. Ablation study on the effects of the three training stages.

| Stage I | Stage II | Stage III | AI2D | MME-S | MMB | GenEval |
|---------|----------|-----------|-------------|---------------|-------------|-------------|
| ✗ | ✓ | ✓ | 78.8 | 1722.3 | 75.3 | 0.82 |
| ✓ | ✗ | ✓ | 75.4 | 1578.9 | 73.2 | 0.77 |
| ✓ | ✓ | ✗ | - | - | - | 0.84 |
| ✓ | ✓ | ✓ | 79.4 | 1877.9 | 76.8 | 0.86 |

across reconstruction fidelity (lowest PSNR, highest rFID), generative capability (lowest GenEval Score), and understanding (Avg QA). Similarly, the 16 + 8 configuration also yields suboptimal results across these metrics compared to the balanced approach. Consequently, the 12 + 12 configuration clearly emerges as the architectural "sweet spot." It achieves peak performance across all evaluated metrics (highest PSNR, Avg QA, and GenEval Score), effectively harmonizing the depth required for semantic abstraction with the structural stability needed for generation.

RQ2: High-Fidelity Reconstruction. We next verify whether our pure ViT-based HYDRA-TOK can serve as a high-quality visual foundation. Historically, ViTs were deemed unsuitable for dense pixel-level synthesis compared to Convolutional VAEs. Tab. 1 challenges this assumption. HYDRA-TOK achieves a PSNR of 36.39 and an rFID of 0.08 on ImageNet-1K (Russakovsky et al., 2014). This performance significantly outperforms unified baselines like BLIP3-o (14.71 PSNR) (Chen et al., 2025a) and even sur-

passes specialized generative tokenizers such as FLUX-VAE (32.74 PSNR) (Labs et al., 2025). This confirms that our *functionally progressive design* (specifically the Gen-ViT) successfully captures compact structure-preserving primitives, allowing a pure ViT to supersede traditional VAEs as a universal visual tokenizer.

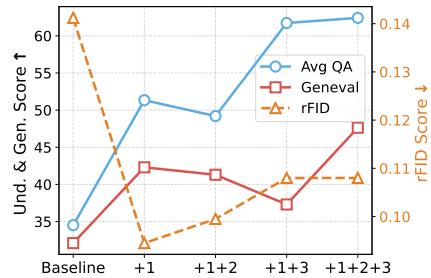


Figure 6. Ablation study of HYDRA-TOK loss components. Baseline utilizes only reconstruction loss (\mathcal{L}_{rec}). Symbols denote additional components: "1": Teacher ViT initialization; "2": Regularization loss (\mathcal{L}_{reg}); "3": Distillation loss (\mathcal{L}_{dist}).

RQ3: Coherence of Information Flow. We assess the coherence of information flow by evaluating multimodal understanding performance, as shown in Tab. 2. Sequential architectures, such as Show-o2 (Xie et al., 2025a), often compromise information coherence due to the compression bottleneck imposed by VAEs. In contrast, HYDRA maintains a continuous and uncompressed information flow

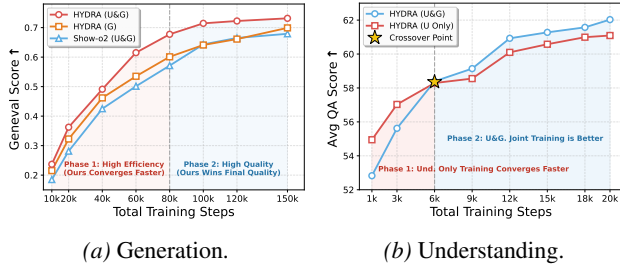


Figure 7. Analysis of representation-harmonized co-promotion. (a) For generation, joint training enhances generation efficiency by stabilizing the latent space. (b) For understanding, joint training surpasses single-task baselines after a crossover point, showing that generative constraints refine perceptual precision. Details of each understanding benchmark and experiment setting is shown in Fig. 10 and Appendix D.2

throughout its pure ViT backbone. At the 1.5B scale, HYDRA demonstrates dominant performance with an average score of 63.1, surpassing the strong baseline Show-o2 (53.2) by a significant margin. This advantage is particularly pronounced in fine-grained tasks sensitive to information loss, such as OCRBench (Liu et al., 2024b), where HYDRA achieves 50.8, a score more than double that of Show-o2 (24.5). Scaling up to 7B, HYDRA continues to lead, outperforming Show-o2 on complex reasoning benchmarks like MMStar (Chen et al., 2024a) (62.3 vs. 56.6) and SEED (Li et al., 2023a) (75.5 vs. 69.8). Most notably, in OCRBench (Liu et al., 2024b), HYDRA preserves high-frequency character details often discarded by VAE-based unified models, scoring 57.7 compared to 32.4 for Show-o2.

RQ4: Compatibility of Generation Learning Process.

We begin by investigating the mechanism behind this compatibility through the training dynamics illustrated in Fig. 8. First, regarding generative harmony (Fig. 7a), we observe that joint training (U&G) consistently outperforms single-task generation (G Only). It not only demonstrates higher convergence efficiency in the early stage (Phase 1) but also achieves superior final fidelity (Phase 2). This validates that the semantic alignment provided by understanding tasks effectively stabilizes the generative latent space, leading to faster and better convergence. Second, regarding understanding harmony (Fig. 7b), a distinct trend appears. While single-task understanding (U Only) learns faster initially, joint training (U&G) overtakes it after a critical *crossover point* (~6k steps). This phenomenon demonstrates that although generation tasks are harder to optimize initially, their fine-grained structural constraints eventually refine the model’s perceptual precision, proving that generation and understanding are mutually reinforcing in our framework.

Supported by this harmonized training dynamic, we further validate the learning compatibility on text-to-image generation benchmarks in Tab. 3. A common failure mode in

UMMs is the “tug-of-war” where improving understanding degrades generation. HYDRA breaks this trade-off, demonstrating that joint optimization leads to superior generative performance. At the 1.5B scale, HYDRA establishes a new benchmark for native UMMs, achieving an Overall GenEval score of 0.86 and DPG-Bench score of 85.51, significantly outperforming Show-o2 (0.73 / 85.02). At the 7B scale, HYDRA sets new state-of-the-art records with a GenEval Overall score of 0.86, surpassing both the unified model Ming-UniVision (Huang et al., 2025) (0.85) and the specialized 12B model FLUX.1 [Dev] (0.82) (Labs et al., 2025). Furthermore, on the WISE benchmark, HYDRA achieves an overall score of 0.53, demonstrating robust alignment across diverse cultural and spatial contexts compared to existing native unified baselines.

3.2. Ablation Analysis

HYDRA-TOK Training Objectives. Fig. 6 validates our tokenizer’s training objectives. The baseline, relying solely on reconstruction loss (\mathcal{L}_{rec}), suffers feature collapse and yields suboptimal results. Teacher initialization provides a crucial semantic scaffold, boosting performance, while distillation (\mathcal{L}_{dist}) further enhances comprehension without compromising structure. Ultimately, the complete objective achieves optimal synergy, balancing understanding, generation, and reconstruction to robustly support the unified architecture.

HYDRA Training Stages. Tab. 4 confirms the indispensability of each stage in our progressive training recipe. Omitting Stage I causes a universal performance decline, underscoring its role in initial alignment. Removing Stage II severely degrades generation while impairing understanding, proving it critical for consolidating the unified feature space. Skipping Stage III results in a total loss of instruction-following capabilities for QA tasks. Consequently, the full recipe yields peak performance across all benchmarks.

4. Conclusion

In this work, we present HYDRA-TOK and HYDRA to reconcile the intrinsic conflict between visual understanding and generation. By employing the Generation-Semantic Bottleneck, HYDRA-TOK functions as a progressive learner that harmonizes structural primitives with semantic abstractions, effectively achieving the *Unification of Input Representation*. This cohesive foundation enables HYDRA to integrate understanding and generation within a single parameter space, satisfying the critical criteria of *Coherence of Information Flow* and *Compatibility of Learning Process*. Our extensive experiments not only establish new state-of-the-art benchmarks but also reveal a fundamental insight: understanding and generation are not competitive objectives

but complementary forces that drive mutual enhancement through rational unification. We believe this representation-harmonized paradigm establishes a new standard for native UMMs, offering a promising trajectory toward more versatile and scalable multimodal intelligence.

Impact Statement

This paper presents work whose goal is to advance the field of Machine Learning, specifically addressing fundamental challenges in creating Unified Multimodal Models that seamlessly integrate visual understanding and generation within a single parameter space. By introducing a representation-harmonized framework that achieves state-of-the-art performance across diverse reconstruction, generation, and understanding benchmarks, our approach contributes to the development of more coherent, capable, and potentially parameter-efficient multimodal AI systems. There are many potential societal consequences of our work, none of which we feel must be specifically highlighted here.

References

- Bai, J., Bai, S., Chu, Y., Cui, Z., Dang, K., Deng, X., Fan, Y., Ge, W., Han, Y., Huang, F., et al. Qwen technical report. *arXiv preprint arXiv:2309.16609*, 2023.
- Byeon, M., Park, B., Kim, H., Lee, S., Baek, W., and Kim, S. Coyo-700m: Image-text pair dataset. <https://github.com/kakaobrain/coyo-dataset>, 2022.
- Cao, S., Chen, H., Chen, P., Cheng, Y., Cui, Y., Deng, X., Dong, Y., Gong, K., Gu, T., Gu, X., et al. Hunyuanimage 3.0 technical report. *arXiv preprint arXiv:2509.23951*, 2025.
- Changpinyo, S., Sharma, P., Ding, N., and Soricut, R. Conceptual 12m: Pushing web-scale image-text pre-training to recognize long-tail visual concepts. In *Proceedings of the IEEE/CVF conference on computer vision and pattern recognition*, pp. 3558–3568, 2021.
- Chen, J., Xu, Z., Pan, X., Hu, Y., Qin, C., Goldstein, T., Huang, L., Zhou, T., Xie, S., Savarese, S., et al. Blip3-o: A family of fully open unified multimodal models-architecture, training and dataset. *arXiv preprint arXiv:2505.09568*, 2025a.
- Chen, L., Li, J., Dong, X., Zhang, P., Zang, Y., Chen, Z., Duan, H., Wang, J., Qiao, Y., Lin, D., et al. Are we on the right way for evaluating large vision-language models? *Advances in Neural Information Processing Systems*, 37: 27056–27087, 2024a.
- Chen, X., Wu, Z., Liu, X., Pan, Z., Liu, W., Xie, Z., Yu, X., and Ruan, C. Janus-pro: Unified multimodal understanding and generation with data and model scaling. *arXiv preprint arXiv:2501.17811*, 2025b.
- Chen, Z., Wang, W., Cao, Y., Liu, Y., Gao, Z., Cui, E., Zhu, J., Ye, S., Tian, H., Liu, Z., et al. Expanding performance boundaries of open-source multimodal models with model, data, and test-time scaling. *arXiv preprint arXiv:2412.05271*, 2024b.
- Chen, Z., Wu, J., Wang, W., Su, W., Chen, G., Xing, S., Zhong, M., Zhang, Q., Zhu, X., Lu, L., et al. Internvl: Scaling up vision foundation models and aligning for generic visual-linguistic tasks. In *Proceedings of the IEEE/CVF Conference on Computer Vision and Pattern Recognition*, pp. 24185–24198, 2024c.
- Deng, C., Zhu, D., Li, K., Gou, C., Li, F., Wang, Z., Zhong, S., Yu, W., Nie, X., Song, Z., et al. Emerging properties in unified multimodal pretraining. *arXiv preprint arXiv:2505.14683*, 2025a.
- Deng, C., Zhu, D., Li, K., Gou, C., Li, F., Wang, Z., Zhong, S., Yu, W., Nie, X., Song, Z., et al. Emerging properties in unified multimodal pretraining. *arXiv preprint arXiv:2505.14683*, 2025b.
- Esser, P., Kulal, S., Blattmann, A., Entezari, R., Müller, J., Saini, H., Levi, Y., Lorenz, D., Sauer, A., Boesel, F., et al. Scaling rectified flow transformers for high-resolution image synthesis. In *Forty-first international conference on machine learning*, 2024.
- Fan, W., Diao, H., Wang, Q., Lin, D., and Liu, Z. The prism hypothesis: Harmonizing semantic and pixel representations via unified autoencoding. *arXiv preprint arXiv:2512.19693*, 2025.
- Fu, C., Chen, P., Shen, Y., Qin, Y., Zhang, M., Lin, X., Yang, J., Zheng, X., Li, K., Sun, X., et al. Mme: A comprehensive evaluation benchmark for multimodal large language models. *arXiv preprint arXiv:2306.13394*, 2023.
- Gadre, S. Y., Ilharco, G., Fang, A., Hayase, J., Smyrnis, G., Nguyen, T., Marten, R., Wortsman, M., Ghosh, D., Zhang, J., et al. Datacomp: In search of the next generation of multimodal datasets. *Advances in Neural Information Processing Systems*, 36:27092–27112, 2023.
- Ge, Y., Zhao, S., Zhu, J., Ge, Y., Yi, K., Song, L., Li, C., Ding, X., and Shan, Y. Seed-x: Multimodal models with unified multi-granularity comprehension and generation. *arXiv preprint arXiv:2404.14396*, 2024.
- Ghosh, D., Hajishirzi, H., and Schmidt, L. Geneval: An object-focused framework for evaluating text-to-image alignment. *Advances in Neural Information Processing Systems*, 36:52132–52152, 2023.

- Gupta, A., Fan, L., Ganguli, S., and Fei-Fei, L. Metamorph: Learning universal controllers with transformers. *arXiv preprint arXiv:2203.11931*, 2022.
- Hu, J., Zhao, S., Chen, Q.-G., Qiu, X., Liu, J., Xu, Z., Luo, W., Zhang, K., and Lu, Y. Omni-view: Unlocking how generation facilitates understanding in unified 3d model based on multiview images. *arXiv preprint arXiv:2511.07222*, 2025.
- Hu, X., Wang, R., Fang, Y., Fu, B., Cheng, P., and Yu, G. Ella: Equip diffusion models with llm for enhanced semantic alignment. *arXiv preprint arXiv:2403.05135*, 2024.
- Huang, Z., Zheng, D., Zou, C., Liu, R., Wang, X., Ji, K., Chai, W., Sun, J., Wang, L., Lv, Y., et al. Ming-univision: Joint image understanding and generation with a unified continuous tokenizer. *arXiv preprint arXiv:2510.06590*, 2025.
- Huh, M., Cheung, B., Wang, T., and Isola, P. The platonic representation hypothesis. *arXiv preprint arXiv:2405.07987*, 2024.
- Jiao, Y., Qiu, H., Jie, Z., Chen, S., Chen, J., Ma, L., and Jiang, Y.-G. Unitoken: Harmonizing multimodal understanding and generation through unified visual encoding. In *Proceedings of the Computer Vision and Pattern Recognition Conference*, pp. 3600–3610, 2025.
- Kembhavi, A., Salvato, M., Kolve, E., Seo, M., Hajishirzi, H., and Farhadi, A. A diagram is worth a dozen images. In *European conference on computer vision*, pp. 235–251. Springer, 2016.
- Kingma, D. P., Welling, M., et al. An introduction to variational autoencoders. *Foundations and Trends® in Machine Learning*, 12(4):307–392, 2019.
- Kirillov, A., Mintun, E., Ravi, N., Mao, H., Rolland, C., Gustafson, L., Xiao, T., Whitehead, S., Berg, A. C., Lo, W.-Y., et al. Segment anything. In *Proceedings of the IEEE/CVF international conference on computer vision*, pp. 4015–4026, 2023.
- Kornblith, S., Norouzi, M., Lee, H., and Hinton, G. Similarity of neural network representations revisited. In *International conference on machine learning*, pp. 3519–3529. PMIR, 2019.
- Labs, B. F., Batifol, S., Blattmann, A., Boesel, F., Consul, S., Diagne, C., Dockhorn, T., English, J., English, Z., Esser, P., et al. Flux. 1 kontekst: Flow matching for in-context image generation and editing in latent space. *arXiv preprint arXiv:2506.15742*, 2025.
- Li, B., Wang, R., Wang, G., Ge, Y., Ge, Y., and Shan, Y. Seed-bench: Benchmarking multimodal llms with generative comprehension. *arXiv preprint arXiv:2307.16125*, 2023a.
- Li, B., Zhang, Y., Guo, D., Zhang, R., Li, F., Zhang, H., Zhang, K., Zhang, P., Li, Y., Liu, Z., et al. Llava-onevision: Easy visual task transfer. *arXiv preprint arXiv:2408.03326*, 2024a.
- Li, B., Zhang, Y., Guo, D., Zhang, R., Li, F., Zhang, H., Zhang, K., Zhang, P., Li, Y., Liu, Z., et al. Llava-onevision: Easy visual task transfer. *arXiv preprint arXiv:2408.03326*, 2024b.
- Li, J., Zhou, S., Guo, L., Qiu, X., Xu, L., Qu, D., Long, T., Fan, C., Li, M., Fan, H., et al. Uniface: A unified fine-grained face understanding and generation model. *arXiv preprint arXiv:2503.08120*, 2025.
- Li, X., Zhang, F., Diao, H., Wang, Y., Wang, X., and Duan, L. Densefusion-1m: Merging vision experts for comprehensive multimodal perception. *Advances in Neural Information Processing Systems*, 37:18535–18556, 2024c.
- Li, Y., Du, Y., Zhou, K., Wang, J., Zhao, W. X., and Wen, J.-R. Evaluating object hallucination in large vision-language models. *arXiv preprint arXiv:2305.10355*, 2023b.
- Liao, C., Liu, L., Wang, X., Luo, Z., Zhang, X., Zhao, W., Wu, J., Li, L., Tian, Z., and Huang, W. Mogao: An omni foundation model for interleaved multi-modal generation. *arXiv preprint arXiv:2505.05472*, 2025a.
- Liao, C., Liu, L., Wang, X., Luo, Z., Zhang, X., Zhao, W., Wu, J., Li, L., Tian, Z., and Huang, W. Mogao: An omni foundation model for interleaved multi-modal generation. *arXiv preprint arXiv:2505.05472*, 2025b.
- Liu, H., Li, C., Li, Y., and Lee, Y. J. Improved baselines with visual instruction tuning, 2023a.
- Liu, H., Li, C., Wu, Q., and Lee, Y. J. Visual instruction tuning. *Advances in neural information processing systems*, 36:34892–34916, 2023b.
- Liu, Y., Duan, H., Zhang, Y., Li, B., Zhang, S., Zhao, W., Yuan, Y., Wang, J., He, C., Liu, Z., et al. Mmbench: Is your multi-modal model an all-around player? In *European conference on computer vision*, pp. 216–233. Springer, 2024a.
- Liu, Y., Li, Z., Huang, M., Yang, B., Yu, W., Li, C., Yin, X.-C., Liu, C.-L., Jin, L., and Bai, X. Ocrbench: on the hidden mystery of ocr in large multimodal models. *Science China Information Sciences*, 67(12):220102, 2024b.

- Liu, Z., Ren, W., Liu, H., Zhou, Z., Chen, S., Qiu, H., Huang, X., An, Z., Yang, F., Patel, A., et al. Tuna: Taming unified visual representations for native unified multimodal models. *arXiv preprint arXiv:2512.02014*, 2025.
- Loshchilov, I. and Hutter, F. Decoupled weight decay regularization. *arXiv preprint arXiv:1711.05101*, 2017.
- Ma, C., Jiang, Y., Wu, J., Yang, J., Yu, X., Yuan, Z., Peng, B., and Qi, X. Unitok: A unified tokenizer for visual generation and understanding. *arXiv preprint arXiv:2502.20321*, 2025a.
- Ma, C., Jiang, Y., Wu, J., Yang, J., Yu, X., Yuan, Z., Peng, B., and Qi, X. Unitok: A unified tokenizer for visual generation and understanding. *arXiv preprint arXiv:2502.20321*, 2025b.
- Ma, Y., Liu, X., Chen, X., Liu, W., Wu, C., Wu, Z., Pan, Z., Xie, Z., Zhang, H., Yu, X., et al. Janusflow: Harmonizing autoregression and rectified flow for unified multimodal understanding and generation. In *Proceedings of the Computer Vision and Pattern Recognition Conference*, pp. 7739–7751, 2025c.
- Niu, Y., Ning, M., Zheng, M., Jin, W., Lin, B., Jin, P., Liao, J., Feng, C., Ning, K., Zhu, B., et al. Wise: A world knowledge-informed semantic evaluation for text-to-image generation. *arXiv preprint arXiv:2503.07265*, 2025.
- Pan, X., Shukla, S. N., Singh, A., Zhao, Z., Mishra, S. K., Wang, J., Xu, Z., Chen, J., Li, K., Juefei-Xu, F., et al. Transfer between modalities with metaqueries. *arXiv preprint arXiv:2504.06256*, 2025.
- Peebles, W. and Xie, S. Scalable diffusion models with transformers. In *Proceedings of the IEEE/CVF international conference on computer vision*, pp. 4195–4205, 2023.
- Podell, D., English, Z., Lacey, K., Blattmann, A., Dockhorn, T., Müller, J., Penna, J., and Rombach, R. Sdxl: Improving latent diffusion models for high-resolution image synthesis. *arXiv preprint arXiv:2307.01952*, 2023.
- Qu, L., Zhang, H., Liu, Y., Wang, X., Jiang, Y., Gao, Y., Ye, H., Du, D. K., Yuan, Z., and Wu, X. Tokenflow: Unified image tokenizer for multimodal understanding and generation. In *Proceedings of the Computer Vision and Pattern Recognition Conference*, pp. 2545–2555, 2025.
- Radford, A., Kim, J. W., Hallacy, C., Ramesh, A., Goh, G., Agarwal, S., Sastry, G., Askell, A., Mishkin, P., Clark, J., et al. Learning transferable visual models from natural language supervision. In *International conference on machine learning*, pp. 8748–8763. PmLR, 2021.
- Ramesh, A., Pavlov, M., Goh, G., Gray, S., Voss, C., Radford, A., Chen, M., and Sutskever, I. Zero-shot text-to-image generation. *ArXiv*, abs/2102.12092, 2021.
- Rombach, R., Blattmann, A., Lorenz, D., Esser, P., and Ommer, B. High-resolution image synthesis with latent diffusion models. In *Proceedings of the IEEE/CVF conference on computer vision and pattern recognition*, pp. 10684–10695, 2022.
- Russakovsky, O., Deng, J., Su, H., Krause, J., Satheesh, S., Ma, S., Huang, Z., Karpathy, A., Khosla, A., Bernstein, M. S., Berg, A. C., and Fei-Fei, L. Imagenet large scale visual recognition challenge. *International Journal of Computer Vision*, 115:211 – 252, 2014.
- Shaulov, A., Hazan, I., Wolf, L., and Chefer, H. Flowmo: Variance-based flow guidance for coherent motion in video generation. *arXiv preprint arXiv:2506.01144*, 2025.
- Shen, T., Yu, J., Zhou, D., Li, D., and Barsoum, E. Emmdit: Revisiting multimodal diffusion transformer design for fast image synthesis under limited resources. *arXiv preprint arXiv:2510.27135*, 2025.
- Shi, M., Wang, H., Zheng, W., Yuan, Z., Wu, X., Wang, X., Wan, P., Zhou, J., and Lu, J. Latent diffusion model without variational autoencoder. *arXiv preprint arXiv:2510.15301*, 2025.
- Sun, K., Pan, J., Ge, Y., Li, H., Duan, H., Wu, X., Zhang, R., Zhou, A., Qin, Z., Wang, Y., et al. Journeydb: A benchmark for generative image understanding. *Advances in neural information processing systems*, 36:49659–49678, 2023.
- Sun, Q., Cui, Y., Zhang, X., Zhang, F., Yu, Q., Wang, Y., Rao, Y., Liu, J., Huang, T., and Wang, X. Generative multimodal models are in-context learners. In *Proceedings of the IEEE/CVF Conference on Computer Vision and Pattern Recognition*, pp. 14398–14409, 2024.
- Tang, H., Xie, C., Bao, X., Weng, T., Li, P., Zheng, Y., and Wang, L. Unilip: Adapting clip for unified multimodal understanding, generation and editing. *arXiv preprint arXiv:2507.23278*, 2025.
- Tschannen, M., Gritsenko, A., Wang, X., Naeem, M. F., Alabdulmohsin, I., Parthasarathy, N., Evans, T., Beyer, L., Xia, Y., Mustafa, B., et al. Siglip 2: Multilingual vision-language encoders with improved semantic understanding, localization, and dense features. *arXiv preprint arXiv:2502.14786*, 2025.
- Wan, T., Wang, A., Ai, B., Wen, B., Mao, C., Xie, C.-W., Chen, D., Yu, F., Zhao, H., Yang, J., Zeng, J., Wang, J., Zhang, J., Zhou, J., Wang, J., Chen, J., Zhu, K., Zhao,

- K., Yan, K., Huang, L., Feng, M., Zhang, N., Li, P., Wu, P., Chu, R., Feng, R., Zhang, S., Sun, S., Fang, T., Wang, T., Gui, T., Weng, T., Shen, T., Lin, W., Wang, W., Wang, W., Zhou, W., Wang, W., Shen, W., Yu, W., Shi, X., Huang, X., Xu, X., Kou, Y., Lv, Y., Li, Y., Liu, Y., Wang, Y., Zhang, Y., Huang, Y., Li, Y., Wu, Y., Liu, Y., Pan, Y., Zheng, Y., Hong, Y., Shi, Y., Feng, Y., Jiang, Z., Han, Z., Wu, Z.-F., and Liu, Z. Wan: Open and advanced large-scale video generative models. *arXiv preprint arXiv:2503.20314*, 2025.
- Wang, X., Zhang, X., Luo, Z., Sun, Q., Cui, Y., Wang, J., Zhang, F., Wang, Y., Li, Z., Yu, Q., et al. Emu3: Next-token prediction is all you need. *arXiv preprint arXiv:2409.18869*, 2024.
- Wu, C., Chen, X., Wu, Z., Ma, Y., Liu, X., Pan, Z., Liu, W., Xie, Z., Yu, X., Ruan, C., et al. Janus: Decoupling visual encoding for unified multimodal understanding and generation. In *Proceedings of the Computer Vision and Pattern Recognition Conference*, pp. 12966–12977, 2025a.
- Wu, C., Chen, X., Wu, Z., Ma, Y., Liu, X., Pan, Z., Liu, W., Xie, Z., Yu, X., Ruan, C., et al. Janus: Decoupling visual encoding for unified multimodal understanding and generation. In *Proceedings of the Computer Vision and Pattern Recognition Conference*, pp. 12966–12977, 2025b.
- Wu, S., Wu, Z., Gong, Z., Tao, Q., Jin, S., Li, Q., Li, W., and Loy, C. C. Openuni: A simple baseline for unified multimodal understanding and generation. *arXiv preprint arXiv:2505.23661*, 2025c.
- Wu, S., Zhang, W., Xu, L., Jin, S., Wu, Z., Tao, Q., Liu, W., Li, W., and Loy, C. C. Harmonizing visual representations for unified multimodal understanding and generation. *arXiv preprint arXiv:2503.21979*, 2025d.
- Wu, Y., Zhang, Z., Chen, J., Tang, H., Li, D., Fang, Y., Zhu, L., Xie, E., Yin, H., Yi, L., et al. Vila-u: a unified foundation model integrating visual understanding and generation. *arXiv preprint arXiv:2409.04429*, 2024.
- Xie, J., Mao, W., Bai, Z., Zhang, D. J., Wang, W., Lin, K. Q., Gu, Y., Chen, Z., Yang, Z., and Shou, M. Z. Show-o: One single transformer to unify multimodal understanding and generation. *arXiv preprint arXiv:2408.12528*, 2024.
- Xie, J., Yang, Z., and Shou, M. Z. Show-o2: Improved native unified multimodal models. *arXiv preprint arXiv:2506.15564*, 2025a.
- Xie, R., Du, C., Song, P., and Liu, C. Muse-vl: Modeling unified vlm through semantic discrete encoding. In *Proceedings of the IEEE/CVF International Conference on Computer Vision*, pp. 24135–24146, 2025b.
- Yang, A., Yang, B., Zhang, B., Hui, B., Zheng, B., Yu, B., Li, C., Liu, D., Huang, F., Wei, H., Lin, H., Yang, J., Tu, J., Zhang, J., Yang, J., Yang, J., Zhou, J., Lin, J., Dang, K., Lu, K., Bao, K., Yang, K., Yu, L., Li, M., Xue, M., Zhang, P., Zhu, Q., Men, R., Lin, R., Li, T., Xia, T., Ren, X., Ren, X., Fan, Y., Su, Y., Zhang, Y., Wan, Y., Liu, Y., Cui, Z., Zhang, Z., and Qiu, Z. Qwen2.5 technical report. *arXiv preprint arXiv:2412.15115*, 2024.
- Yao, J., Song, Y., Zhou, Y., and Wang, X. Towards scalable pre-training of visual tokenizers for generation. *arXiv preprint arXiv:2512.13687*, 2025a.
- Yao, J., Yang, B., and Wang, X. Reconstruction vs. generation: Taming optimization dilemma in latent diffusion models. In *Proceedings of the Computer Vision and Pattern Recognition Conference*, pp. 15703–15712, 2025b.
- Yu, S., Kwak, S., Jang, H., Jeong, J., Huang, J., Shin, J., and Xie, S. Representation alignment for generation: Training diffusion transformers is easier than you think. *arXiv preprint arXiv:2410.06940*, 2024.
- Yue, X., Ni, Y., Zhang, K., Zheng, T., Liu, R., Zhang, G., Stevens, S., Jiang, D., Ren, W., Sun, Y., et al. Mmmu: A massive multi-discipline multimodal understanding and reasoning benchmark for expert agi. In *Proceedings of the IEEE/CVF Conference on Computer Vision and Pattern Recognition*, pp. 9556–9567, 2024.
- Yue, Z., Zhang, H., Zeng, X., Chen, B., Wang, C., Zhuang, S., Dong, L., Du, K., Wang, Y., Wang, L., et al. Uniflow: A unified pixel flow tokenizer for visual understanding and generation. *arXiv preprint arXiv:2510.10575*, 2025.
- Zhao, Y., Xue, F., Reed, S., Fan, L., Zhu, Y., Kautz, J., Yu, Z., Krähenbühl, P., and Huang, D.-A. Qlip: Text-aligned visual tokenization unifies auto-regressive multimodal understanding and generation. *arXiv preprint arXiv:2502.05178*, 2025.
- Zheng, B., Ma, N., Tong, S., and Xie, S. Diffusion transformers with representation autoencoders. *arXiv preprint arXiv:2510.11690*, 2025.
- Zhou, C., Yu, L., Babu, A., Tirumala, K., Yasunaga, M., Shamis, L., Kahn, J., Ma, X., Zettlemoyer, L., and Levy, O. Transfusion: Predict the next token and diffuse images with one multi-modal model. *arXiv preprint arXiv:2408.11039*, 2024.

A. Related Works

A.1. Unified Multimodal Models

The pursuit of a singular architecture for both visual understanding and generation has led to the evolution of Unified Multimodal Models (UMMs) (Liao et al., 2025a; Deng et al., 2025b; Hu et al., 2025; Li et al., 2025), broadly categorized into composite and native architectures.

Composite UMMs such as MetaQuery (Gupta et al., 2022), BLIP-3o (Chen et al., 2025a), OpenUni (Wu et al., 2025c) and Unilip (Tang et al., 2025) achieve capability extension by integrating specialized, pre-trained experts (e.g., separate LLMs and Diffusion models) via lightweight adapters. While effective for rapid deployment, their reliance on frozen backbones restricts deep inter-modal interaction, resulting in a shallow unification where understanding and generation remain functionally decoupled.

Native UMMs strive for deeper integration by training holistically within a shared parameter space. However, as analyzed in Fig. 2, existing methods are constrained by a fundamental representation trilemma: (i) Decoupled Architectures, such as the Janus series (Wu et al., 2025b; Ma et al., 2025c), Bagel (Deng et al., 2025a) and UniToken (Jiao et al., 2025), mitigate task interference by utilizing separate or dual encoders for vision and language. While UniToken concatenates discrete and continuous tokens to bridge modalities, this dual-encoder design inherently sacrifices *Unification of Input Representation*, leading to parameter redundancy, computational inefficiency due to sequence inflation, and severed task synergy. (ii) Sequential Architectures, including Show-o2 (Xie et al., 2025a) and TUNA (Liu et al., 2025), attempt to unify inputs by stacking semantic encoders atop a VAE. However, the heavy compression required for the VAE acts as an information bottleneck, disrupting the *Coherence of Information Flow* and diluting the fine-grained structural signals needed for generation. (iii) Shared Architectures, such as Unitok (Ma et al., 2025b) and Transfusion (Zhou et al., 2024; Wu et al., 2025d), attempt to unify tasks but struggle with the *Compatibility of Learning Process*. On one hand, discrete approaches like Unitok (Ma et al., 2025b) suffer from quantization errors inherent in codebooks, which fundamentally conflict with the high-fidelity requirements of synthesis. On the other hand, continuous approaches like Transfusion (Zhou et al., 2024) and Harmon (Wu et al., 2025d) employ VAE latent features for both tasks; while these representations are adequate for generation, they lack the high-dimensional semantic abstractions required for perception, resulting in suboptimal performance on complex understanding tasks. In contrast, our HYDRA achieves rational unification by resolving these conflicts through a harmonized, continuous representation.

A.2. Unified Tokenizers and Representations

Recent research has shifted from discrete to continuous unified representations to bridge the gap between semantic abstraction and pixel-level fidelity. To circumvent the traditional variational bottleneck, paradigms such as RAE (Zheng et al., 2025) and SVG (Shi et al., 2025) employ frozen, pre-trained semantic encoders. While this accelerates convergence, the inherent loss of low-level features compromises reconstruction fidelity. Although UniFlow (Yue et al., 2025) attempts to recover structural details via self-distillation, it relies on dual-stream features, failing to achieve a truly unified, single-stream information flow. Similarly, QLIP (Zhao et al., 2025) seeks to unify representations by aligning visual tokens with textual semantics; however, this heavy reliance on linguistic alignment imposes a semantic bottleneck, filtering out the high-frequency textural details necessary for photorealistic synthesis. Furthermore, while VTP (Yao et al., 2025a) improves generative scaling by jointly optimizing contrastive and reconstruction losses, its low-dimensional latent space is tailored for generation and lacks the representational capacity required for complex multimodal perception. Distinctly, our HYDRA-TOK employs a functionally progressive pure ViT backbone to actively bridge the representation gap. This design ensures a coherent single-stream flow, eliminating quantization errors while simultaneously satisfying the conflicting demands of high-fidelity synthesis and deep semantic understanding.

B. Limitations and Future Work

Despite establishing promising benchmarks, our current implementation faces limitations in scale that define future research directions. A primary constraint is the 300M parameter HYDRA-TOK, which creates a potential bottleneck for encoding intricate details in fine-grained tasks. Furthermore, relying on a 7B parameter model trained on only 100M image-text pairs restricts generalizability and world knowledge absorption compared to state-of-the-art foundation models. Consequently, our immediate future work will center on significantly scaling both the model architecture and the training dataset size to address these gaps and unlock robust capabilities across diverse multimodal tasks.

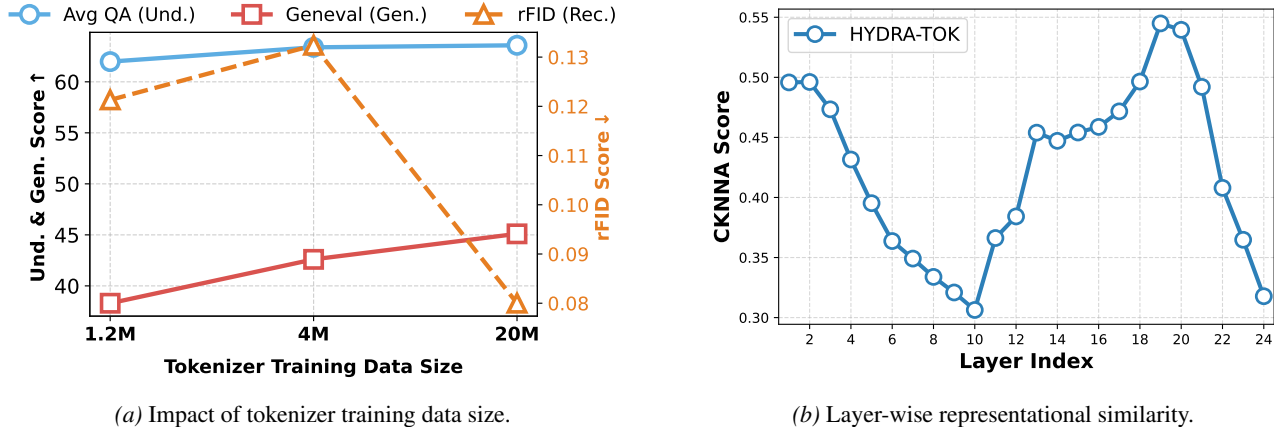


Figure 8. Analysis of tokenizer data scaling and layer-wise representations. (a) This figure illustrates how understanding (Avg QA), generation (Geneval), and reconstruction (rFID) metrics evolve as the tokenizer training data size increases from 1.2M to 20M. (b) The figure shows the CKNNA score across the 24 layers of the HYDRA-TOK, indicating the change in representational similarity between teacher vit (Chen et al., 2024b).

C. Additional ablation study results

C.1. Decoder Size

We investigate the impact of decoder parameter size on the visual reconstruction quality. Tab. 5 presents a quantitative comparison across three different decoder capacities ranging from approximately 144M to 358M parameters. We observe a clear trend where increasing the decoder size leads to monotonic improvements across all evaluated metrics. Specifically, scaling the decoder from 144.26M to 358.44M results in a 0.99 dB increase in PSNR (from 35.85 to 36.84), a 0.01 improvement in SSIM (from 0.96 to 0.97), and a notable decrease in rFID from 0.17 to 0.15. The largest model variant (358.44M) consistently achieves the best performance, demonstrating that larger decoder capacities are beneficial for achieving high-fidelity visual reconstruction.

Table 5. Quantitative comparison of reconstruction quality across different model variants.

| Decoder Size | PSNR \uparrow | SSIM \uparrow | rFID \downarrow |
|--------------|-----------------|-----------------|-------------------|
| 144.26M | 35.85 | 0.96 | 0.17 |
| 240.85M | 36.55 | 0.96 | 0.15 |
| 358.44M | 36.84 | 0.96 | 0.15 |

C.2. Scaling HYDRA-TOK training data

For multimodal understanding capabilities, the tokenizer is trained utilizing the LLaVA-1.5 setting (Liu et al., 2023a). As illustrated in Fig. 8a, we evaluate performance across three data regimes: 1.2M, 4M, and 20M image-text pairs. The evaluation metrics include generation (Geneval), reconstruction (rFID), and understanding (Avg QA), where Avg QA denotes the average score across the POPE (Li et al., 2023b), MMBench (Liu et al., 2024a), MMMU (Yue et al., 2024), AI2D (Kembhavi et al., 2016), and RealWorldQA benchmarks. We observe distinct trends for different capabilities as the data size increases. The generative capability, indicated by the Geneval score, shows a consistent positive trend, improving steadily from approximately 38 at 1.2M to over 45 when trained on 20M data. Reconstruction fidelity, measured by rFID (where lower is better), also benefits significantly from larger data scales. While it shows a slight increase at 4M, it achieves its best performance with a sharp drop to approximately 0.08 at the 20M mark. Conversely, multimodal understanding capabilities, as reflected by the Avg QA score, remain relatively stable and robust across all data sizes, maintaining a score consistently above 61. These results suggest that while understanding capabilities are established early, scaling the tokenizer training data is critical for optimizing generation and reconstruction performance.

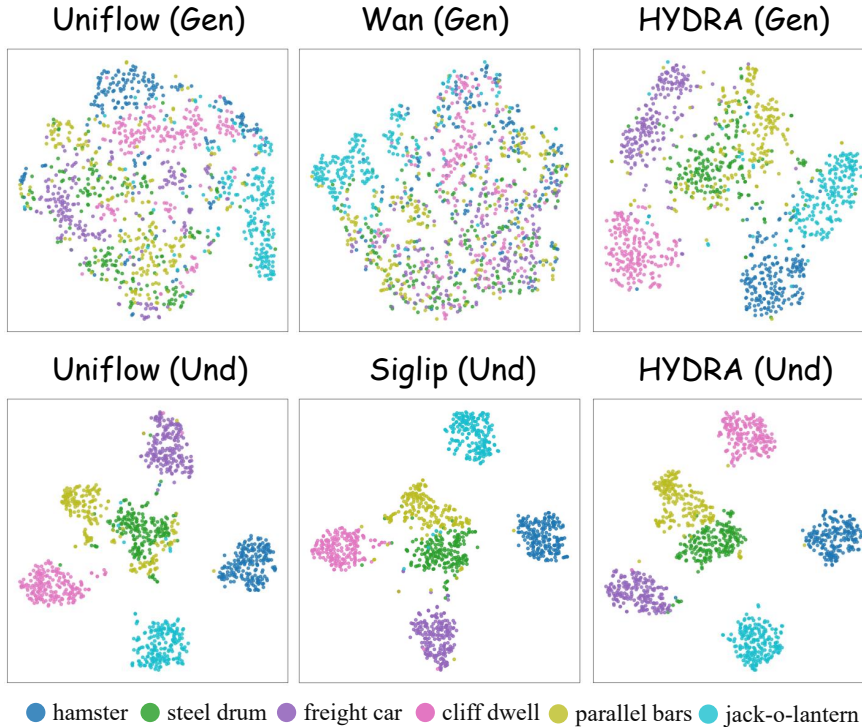


Figure 9. Qualitative comparison of t-SNE.

C.3. Visualization of CKNNA

To better illustrate the coherence of information flow within our model, we conducted a representational similarity analysis using Centered Kernel Nearest-Neighbor Alignment (CKNNA) (Huh et al., 2024). We randomly selected 10,000 images from the ImageNet2012 validation set (Russakovsky et al., 2014) to calculate the CKNNA metric between our HYDRA-TOK and the teacher model, InternViT. As observed in Fig. 8b, our model exhibits strong alignment in early layers.

Simultaneously, we calculated the CKNNA index between the generation features and understanding features within our model. Our model achieves a score of 0.10, which is significantly higher than the 0.03 achieved by the Show-o2 model. This indicates a highly coherent transition between generation and understanding feature representations in our approach. Furthermore, we observe that as unified training progresses, this metric continuously increases, eventually reaching 0.13.

C.4. Visualization of t-SNE

As shown in Fig. 9, we visualize the learned features from both the generation and understanding branches of HYDRA, comparing them against UniFlow (Yue et al., 2025) and Show-o2 (Xie et al., 2025a) (equipped with WAN (Wan et al., 2025) and SigLIP (Tschannen et al., 2025)). While the baselines often exhibit disparately distributed features, HYDRA demonstrates distinct class clusters in both its generation and understanding representations. This strong semantic discriminability indicates a high degree of alignment between the two feature spaces. Such similarity confirms that our architecture establishes a coherent information flow, enabling the two tasks to be collaboratively optimized within a harmonized representational framework.

D. Training details

HYDRA-TOK is training in two progressive stages to effectively balance representation learning and generative quality. Stage 1: Foundation Training. In the initial stage, we focus on establishing the foundational capabilities of the tokenizer through joint reconstruction and distillation objectives. We utilize a large-scale composite dataset consisting of ImageNet-1.2M, CC-12M, and SAM-10M. During this phase, the entire tokenizer (both encoder and decoder) is trained end-to-end. We optimize the model for a total of 300k iterations with a global batch size of 256. The learning rate is set to $2e - 5$.

Stage 2: Decoder Refinement. In the second stage, we shift our focus to refining the fidelity of the generated images. We freeze the parameters of the pre-trained encoder to preserve the learned semantic representations and exclusively fine-tune the decoder. In this phase, the distillation objective is discarded. Instead, we incorporate adversarial training (GAN loss) alongside the reconstruction loss to enhance perceptual quality. The learning rate is reduced to , and the training proceeds for an additional 100k iterations.

HYDRA training proceeds through a progressive three-stage curriculum, with specific hyperparameters detailed in Tab. 6. Across all three stages, we maintain a constant input image resolution of 448×448 and a global batch size of 1024. We employ varying learning rates (LRs) tailored to different model components and training phases. In Stage I, the Vision Head and Sem-ViT are trained with LRs of 10^{-4} and 5×10^{-5} , respectively. Progressing to Stages II and III, the Vision Head LR is reduced to 5×10^{-5} , while the LLM and Sem-ViT are trained jointly at a lower rate of 2×10^{-5} . The training strategy also involves shifting data mixing ratios and durations: Stage I utilizes a data ratio of 0:1:3 for 150K steps; Stage II adjusts the ratio to 0:2:2 for 100K steps; and Stage III concludes with a ratio of 1:2:2 for 20K steps.

Table 6. Training details of our HYDRA.

| Setting | Stage I | Stage II | Stage III |
|---------------|---|--|--|
| LR. | Vision Head: 10^{-4} Sem-ViT: 5×10^{-5} | Vision Head: 5×10^{-5} LLM & Sem-ViT: 2×10^{-5} | Vision Head: 5×10^{-5} LLM & Sem-ViT: 2×10^{-5} |
| Image Size | 448 | 448 | 448 |
| Batch Size | 1024 | 1024 | 1024 |
| Data Ratio | 0:1:3 | 0:2:2 | 1:2:2 |
| Training Step | 150K | 100K | 20K |

D.1. Ablation study training details

In our ablation studies, the evaluation covers three core capabilities with specific setups: (i) Multimodal Understanding: Following the LLaVA-1.5 training protocol (Liu et al., 2023a), we report the average score (Avg QA) across POPE (Li et al., 2023b), MMBench (Liu et al., 2024a), MMMU (Yue et al., 2024), AI2D (Kembhavi et al., 2016), and RealWorldQA. (ii) Image Generation: We adapt the Nitro-E framework (Shen et al., 2025) by replacing its VAE with our HYDRA-TOK. We train this setup for 15k iterations using the SAM-1B (Kirillov et al., 2023) and JourneyDB (Sun et al., 2023) datasets and evaluate performance on GenEval. (iii) Image Reconstruction: We train on the ImageNet-1k (1.2M) dataset (Russakovsky et al., 2014) for 150k iterations and assess quality using rFID.

D.2. Representation-harmonized co-promotion experiment training details

To validate the mutual benefits of our harmonized representation, we conducted comparative experiments on both generation and understanding tasks. For generation, we trained both Show-o2 and our HYDRA on the same 100M dataset for 150K steps, comparing the GenEval performance of joint training against a generation-only baseline across different training stages. For understanding, we performed Stage III training for 20K steps, comparing joint training with an understanding-only approach. We evaluated the models on general understanding (SEED-Bench), reasoning (MMStar, MMMU, MMBench, AI2D), and OCR-related tasks (OCRBench). Detailed settings for each benchmark are illustrated in Fig. 10.

D.3. Training data

D.3.1. IMAGE UNDERSTANDING

Stage I. For the initial pre-training stage, we utilized a massive dataset comprising approximately 22M images paired with captions. These data were sourced from a diverse collection of large-scale datasets, including ImageNet (Russakovsky et al., 2014), DataComp-1B (Gadre et al., 2023), COYO-700M (Byeon et al., 2022), SA-1B (Kirillov et al., 2023), and DenseFusion (Li et al., 2024c).

Stage II. In Stage II, we continued to utilize the comprehensive collection of data from the sources employed in Stage I (ImageNet (Russakovsky et al., 2014), DataComp-1B (Gadre et al., 2023), COYO-700M (Byeon et al., 2022), SA-1B (Kirillov et al., 2023), and DenseFusion (Li et al., 2024c)) for further training.

Table 7. Detailed image generation results on the GenEval benchmark. † refers to finetuning with GPT-4o distilled dataset (Chen et al., 2025a).

| Models | Size | Single Object | Two Objects | Count | Colors | Position | Color Attribute | Overall |
|---|------|---------------|-------------|-------------|-------------|-------------|-----------------|-------------|
| <i>Generation-only Models</i> | | | | | | | | |
| SD3-Med (Esser et al., 2024) | 2B | 0.99 | 0.94 | 0.72 | 0.89 | 0.33 | 0.60 | 0.74 |
| FLUX.1 [Dev] (Labs et al., 2025) | 12B | 0.98 | 0.93 | 0.75 | 0.93 | 0.68 | 0.65 | 0.82 |
| DALL-E 3 (Ramesh et al., 2021) | - | 0.96 | 0.87 | 0.47 | 0.83 | 0.43 | 0.45 | 0.67 |
| <i>Composite Unified Multimodal Models</i> | | | | | | | | |
| TokenFlow-XL (Qu et al., 2025) | 14B | 0.95 | 0.60 | 0.41 | 0.81 | 0.16 | 0.24 | 0.55 |
| SEED-X (Ge et al., 2024) | 17B | 0.97 | 0.58 | 0.26 | 0.80 | 0.19 | 0.14 | 0.49 |
| MetaQuery-XL (Pan et al., 2025) | 7B | - | - | - | - | - | - | 0.80 |
| Blip3-o † (Chen et al., 2025a) | 8B | - | - | - | - | - | - | 0.84 |
| <i>Smaller Native Unified Multimodal Models</i> | | | | | | | | |
| Show-o (Xie et al., 2024) | 1.3B | 0.95 | 0.52 | 0.49 | 0.82 | 0.11 | 0.28 | 0.53 |
| Harmon (Wu et al., 2025d) | 1.5B | 0.99 | 0.86 | 0.66 | 0.85 | 0.74 | 0.48 | 0.76 |
| Show-o2 (Xie et al., 2025a) | 1.5B | 0.99 | 0.86 | 0.55 | 0.86 | 0.46 | 0.63 | 0.73 |
| HYDRA | 1.5B | 1.00 | 0.95 | 0.75 | 0.91 | 0.76 | 0.77 | 0.86 |
| <i>Larger Native Unified Multimodal Models</i> | | | | | | | | |
| Ming-UniVision (Huang et al., 2025) | 16B | 1.00 | 0.93 | 0.59 | 0.93 | 0.92 | 0.70 | 0.85 |
| BAGEL (Deng et al., 2025b) | 14B | 0.98 | 0.95 | 0.84 | 0.95 | 0.78 | 0.77 | 0.88 |
| MUSE-VL (Xie et al., 2025b) | 7B | 0.98 | 0.64 | 0.54 | 0.72 | 0.25 | 0.31 | 0.57 |
| Janus-Pro (Chen et al., 2025b) | 7B | 0.99 | 0.89 | 0.59 | 0.90 | 0.79 | 0.66 | 0.80 |
| Show-o2 (Xie et al., 2025a) | 7B | 1.00 | 0.87 | 0.58 | 0.92 | 0.52 | 0.62 | 0.76 |
| HYDRA | 7B | 1.00 | 0.97 | 0.68 | 0.91 | 0.81 | 0.80 | 0.86 |

Stage III. For the final high-quality fine-tuning stage, we directly utilized the refined 3.2M instruction-tuning data from LLaVA-One-Vision (Li et al., 2024a) to maximize image understanding performance.

D.3.2. IMAGE GENERATION

Stage I. For the initial generation training stage, we curated a large-scale dataset totaling approximately 78M samples. This comprises SA-1B (Kirillov et al., 2023), CC-12M (Changpinyo et al., 2021), 1M images from DenseFusion (Li et al., 2024c), and an internal dataset consisting of 55M real images.

Stage II. Stage II expands upon the data used in Stage I. In addition to SA-1B (Kirillov et al., 2023), CC-12M (Changpinyo et al., 2021), the 55M internal real images, and DenseFusion-1M (Li et al., 2024c), we incorporated 10M synthetic images generated through Flux distillation, following the methodology described in (Shen et al., 2025).

Stage III. For high-quality generation fine-tuning, we utilized the JourneyDB dataset (Sun et al., 2023) and DenseFusion-1M (Li et al., 2024c). Additionally, we refined the 10M Flux-distilled data from Stage II through filtering, selecting a high-quality subset of 5M images for this final stage.

E. Additional main results

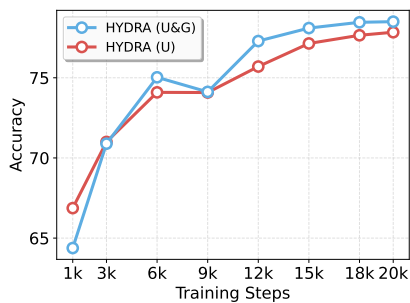
F. Evaluation Details

F.1. Multi-modal Understanding Benchmarks

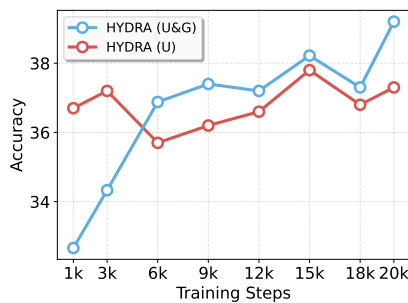
To comprehensively evaluate the perception and reasoning capabilities of HYDRA, we employ eight diverse benchmarks covering general understanding, expert knowledge, and fine-grained visual perception. We utilize MME (Fu et al., 2023) to measure comprehensive perception and cognition, reporting MME-S as the aggregate sum of both scores. MMBench (MMB) (Liu et al., 2024a) is employed for its robust circular evaluation strategy, assessing fine-grained perception and logical reasoning. To ensure rational visual dependency, we evaluate on MMStar (Chen et al., 2024a), a curated benchmark that filters out samples solvable by text alone. Additionally, SEED-Bench (SEED) (Li et al., 2023a) serves as a large-scale testbed for generative and discriminative comprehension across spatial and temporal dimensions. For high-level discipline-specific

Table 8. Detailed image generation results on the DPG-Bench benchmark (Hu et al., 2024).

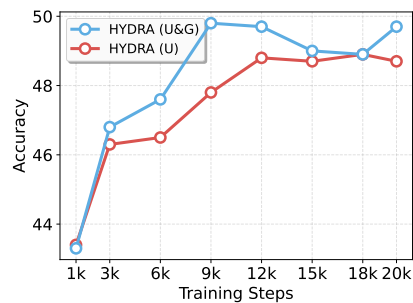
| Models | Size | Global | Entity | Attribute | Relation | Other | Overall |
|---|------|--------------|--------------|--------------|--------------|--------------|--------------|
| <i>Generation-only Models</i> | | | | | | | |
| FLUX.1 [Dev] (Labs et al., 2025) | 12B | 82.10 | 89.50 | 88.70 | 91.10 | 89.40 | 84.00 |
| <i>Smaller Native Unified Multimodal Models</i> | | | | | | | |
| Show-o2 (Xie et al., 2025a) | 1.5B | 87.53 | 90.38 | 91.34 | 90.30 | 91.21 | 85.02 |
| HYDRA | 1.5B | 89.65 | 91.62 | 90.24 | 91.59 | 90.88 | 85.51 |
| <i>Larger Native Unified Multimodal Models</i> | | | | | | | |
| Janus-Pro (Chen et al., 2025b) | 7B | 86.90 | 88.90 | 89.40 | 89.32 | 89.48 | 84.19 |
| BAGEL (Deng et al., 2025b) | 14B | 88.94 | 90.37 | 91.29 | 90.82 | 88.67 | 85.07 |
| Show-o2 (Xie et al., 2025a) | 7B | 89.00 | 91.78 | 89.96 | 91.81 | 91.64 | 86.14 |
| HYDRA | 7B | 90.22 | 91.88 | 89.92 | 91.83 | 90.93 | 86.40 |



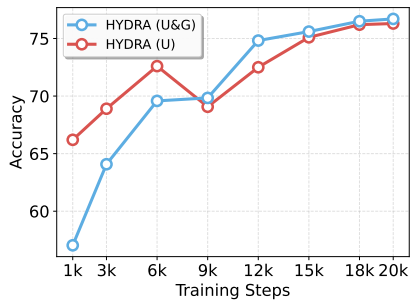
(a) AI2D (Kembhavi et al., 2016).



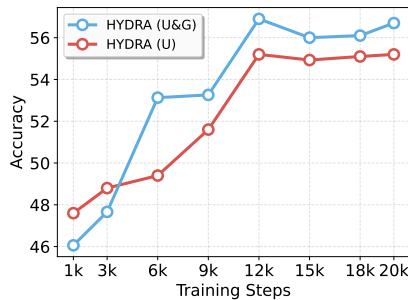
(b) MMMU (Yue et al., 2024).



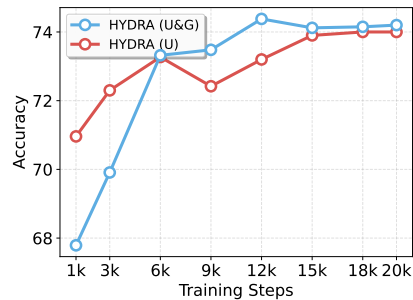
(c) OCRBench (Liu et al., 2024b).



(d) MMBench (Liu et al., 2024a).



(e) MMStar (Chen et al., 2024a).



(f) SEED-Bench (Li et al., 2023a).

Figure 10. Performance comparison on various benchmarks across different training steps. The benchmarks include general perception (SEED-Bench), reasoning (MMStar, MMMU, MMBench, AI2D), and OCR-related tasks (OCRBench).

reasoning, we employ MMMU (Yue et al., 2024), a massive multi-discipline benchmark demanding expert-level reasoning across fields such as art, science, and engineering. This is complemented by AI2D (Kembhavi et al., 2016), a specialized dataset focused on understanding and answering questions about scientific diagrams and textbook illustrations. To assess text-centric visual understanding, we use OCRBench (Liu et al., 2024b), a dedicated benchmark for optical character recognition tasks. Furthermore, RealWorldQA (RWQA) is utilized to evaluate spatial reasoning and physical understanding in diverse real-world environments.

F.2. CKNNA

CKNNA (Centered Kernel Nearest-Neighbor Alignment) is a similarity metric designed to compare representations by emphasizing *local relational structure* rather than global correspondence. Unlike Centered Kernel Alignment (CKA;

Table 9. Detailed image generation results on the WISE benchmark (Niu et al., 2025).

| Models | Size | Culture | Time | Space | Biology | Physics | Chemistry | Overall |
|---|------|-------------|-------------|-------------|-------------|-------------|-------------|-------------|
| <i>Generation-only Models</i> | | | | | | | | |
| FLUX.1 [Dev] (Labs et al., 2025) | 12B | 0.48 | 0.58 | 0.62 | 0.42 | 0.51 | 0.35 | 0.50 |
| SD3.5-Large (Esser et al., 2024) | 8B | 0.44 | 0.50 | 0.58 | 0.44 | 0.52 | 0.31 | 0.46 |
| <i>Composite Unified Multimodal Models</i> | | | | | | | | |
| Blip3-o-4B (Chen et al., 2025a) | 4B | - | - | - | - | - | - | 0.50 |
| <i>Smaller Native Unified Multimodal Models</i> | | | | | | | | |
| Harmon (Wu et al., 2025d) | 1.5B | 0.38 | 0.48 | 0.52 | 0.37 | 0.44 | 0.29 | 0.41 |
| Show-o2 (Xie et al., 2025a) | 1.5B | 0.33 | 0.41 | 0.53 | 0.35 | 0.49 | 0.31 | 0.39 |
| HYDRA | 1.5B | 0.49 | 0.47 | 0.64 | 0.42 | 0.59 | 0.34 | 0.49 |
| <i>Larger Native Unified Multimodal Models</i> | | | | | | | | |
| BAGEL (Deng et al., 2025b) | 14B | 0.44 | 0.55 | 0.68 | 0.44 | 0.60 | 0.39 | 0.52 |
| VILA-U-7B (Wu et al., 2024) | 7B | 0.26 | 0.33 | 0.37 | 0.35 | 0.39 | 0.23 | 0.31 |
| Janus-Pro-7B (Chen et al., 2025b) | 7B | 0.30 | 0.37 | 0.49 | 0.36 | 0.42 | 0.26 | 0.35 |
| Emu3-Gen-8B (Wang et al., 2024) | 8B | 0.34 | 0.45 | 0.48 | 0.41 | 0.45 | 0.27 | 0.39 |
| Show-o2 (Xie et al., 2025a) | 7B | 0.40 | 0.45 | 0.58 | 0.39 | 0.53 | 0.34 | 0.44 |
| HYDRA | 7B | 0.52 | 0.53 | 0.68 | 0.47 | 0.58 | 0.38 | 0.53 |

Kornblith et al. 2019), which aggregates correlations over all sample pairs, CKNNA restricts the comparison to pairs that are mutually close in both representation spaces, thereby providing a more flexible and locality-aware measure. Our formulation follows the core principles introduced in (Huh et al., 2024; Yu et al., 2024), while adopting an equivalent but implementation-aligned presentation.

Consider a shared set of n inputs $\{\mathbf{x}_i\}_{i=1}^n$ processed by two models, producing representations ϕ_i and ψ_i , respectively. Using a linear kernel, we define the corresponding similarity matrices

$$\mathbf{K}_{ij} = \langle \phi_i, \phi_j \rangle, \quad \mathbf{L}_{ij} = \langle \psi_i, \psi_j \rangle. \quad (12)$$

To remove first-order biases, we apply row-wise centering:

$$\bar{\mathbf{K}}_{ij} = \mathbf{K}_{ij} - \frac{1}{n} \sum_{l=1}^n \mathbf{K}_{il}, \quad \bar{\mathbf{L}}_{ij} = \mathbf{L}_{ij} - \frac{1}{n} \sum_{l=1}^n \mathbf{L}_{il}. \quad (13)$$

Local alignment is enforced through a mutual neighborhood constraint. Let $\text{KNN}_{\mathbf{K}}(i; k)$ and $\text{KNN}_{\mathbf{L}}(i; k)$ denote the k nearest neighbors of sample i under kernels \mathbf{K} and \mathbf{L} , respectively. We define a binary mask

$$\mathbf{w}_{ij}^{(k)} = \mathbb{1} \left[j \in \text{KNN}_{\mathbf{K}}(i; k) \wedge j \in \text{KNN}_{\mathbf{L}}(i; k) \wedge i \neq j \right]. \quad (14)$$

Using this mask, we compute a neighborhood-restricted covariance score:

$$S(\mathbf{K}, \mathbf{L}) = \sum_{i=1}^n \sum_{j=1}^n \mathbf{w}_{ij}^{(k)} \bar{\mathbf{K}}_{ij} \bar{\mathbf{L}}_{ij}. \quad (15)$$

Analogously, we define the self-similarity terms

$$S(\mathbf{K}, \mathbf{K}) = \sum_{i,j} \mathbf{w}_{ij}^{(k)} \bar{\mathbf{K}}_{ij}^2, \quad S(\mathbf{L}, \mathbf{L}) = \sum_{i,j} \mathbf{w}_{ij}^{(k)} \bar{\mathbf{L}}_{ij}^2. \quad (16)$$

The final CKNNA score is obtained via normalized local alignment:

$$\text{CKNNA}(\mathbf{K}, \mathbf{L}) = \frac{S(\mathbf{K}, \mathbf{L})}{\sqrt{S(\mathbf{K}, \mathbf{K}) S(\mathbf{L}, \mathbf{L})}}. \quad (17)$$

In practice, we uniformly sample 10,000 images from the ImageNet validation set (Russakovsky et al., 2014) and compute CKNNA with $k = 10$. As observed in (Huh et al., 2024), restricting the comparison to small neighborhoods yields a more sensitive measure of representational agreement.

G. Qualitative comparison

G.1. Image Reconstruction

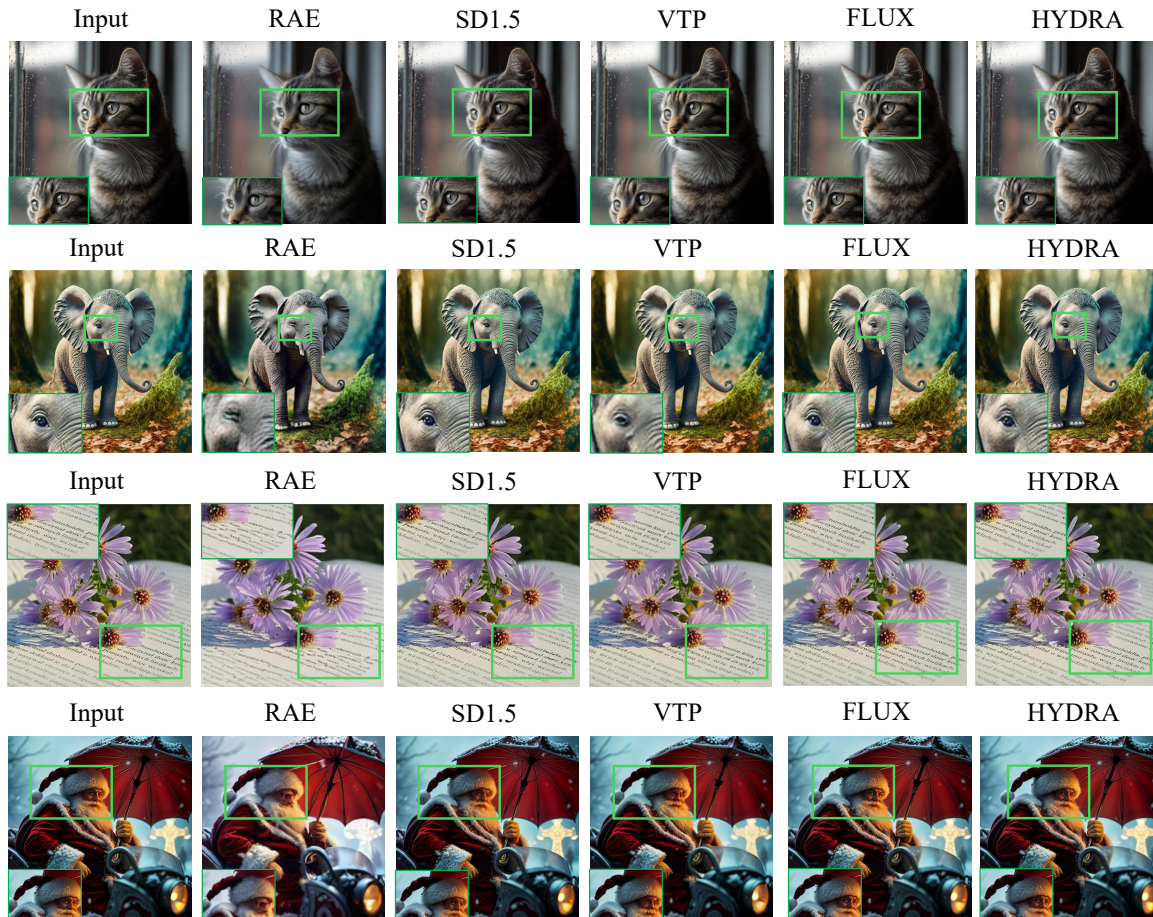


Figure 11. **Qualitative comparison of image reconstruction.** We compare visual results from our HYDRA between RAE (Zheng et al., 2025), SD1.5 (Podell et al., 2023), VTP (Yao et al., 2025a), and FLUX (Labs et al., 2025).

G.2. Image Generation



A clear photo of a classic red stop sign with bold white letters spelling "STOP" in the center.



A detailed photo of a clock hanging on a plain wall.



A photo of a pink stop sign.



Generate an image of a banana and a bunch of grapes, with the yellow fruit on the right side and the purple fruit on the left side.



A citrus fruit known for its sweetness and juiciness, widely cultivated in Spain, especially the Valencia variety.

Figure 12. **Qualitative comparison of text-to-image generation.** We compare visual generation between Harmon (Wu et al., 2025d), Show-o2 (Xie et al., 2025a), Bagel (Deng et al., 2025a), Janus-pro (Wu et al., 2025b), and Blip-3o (Chen et al., 2025a).

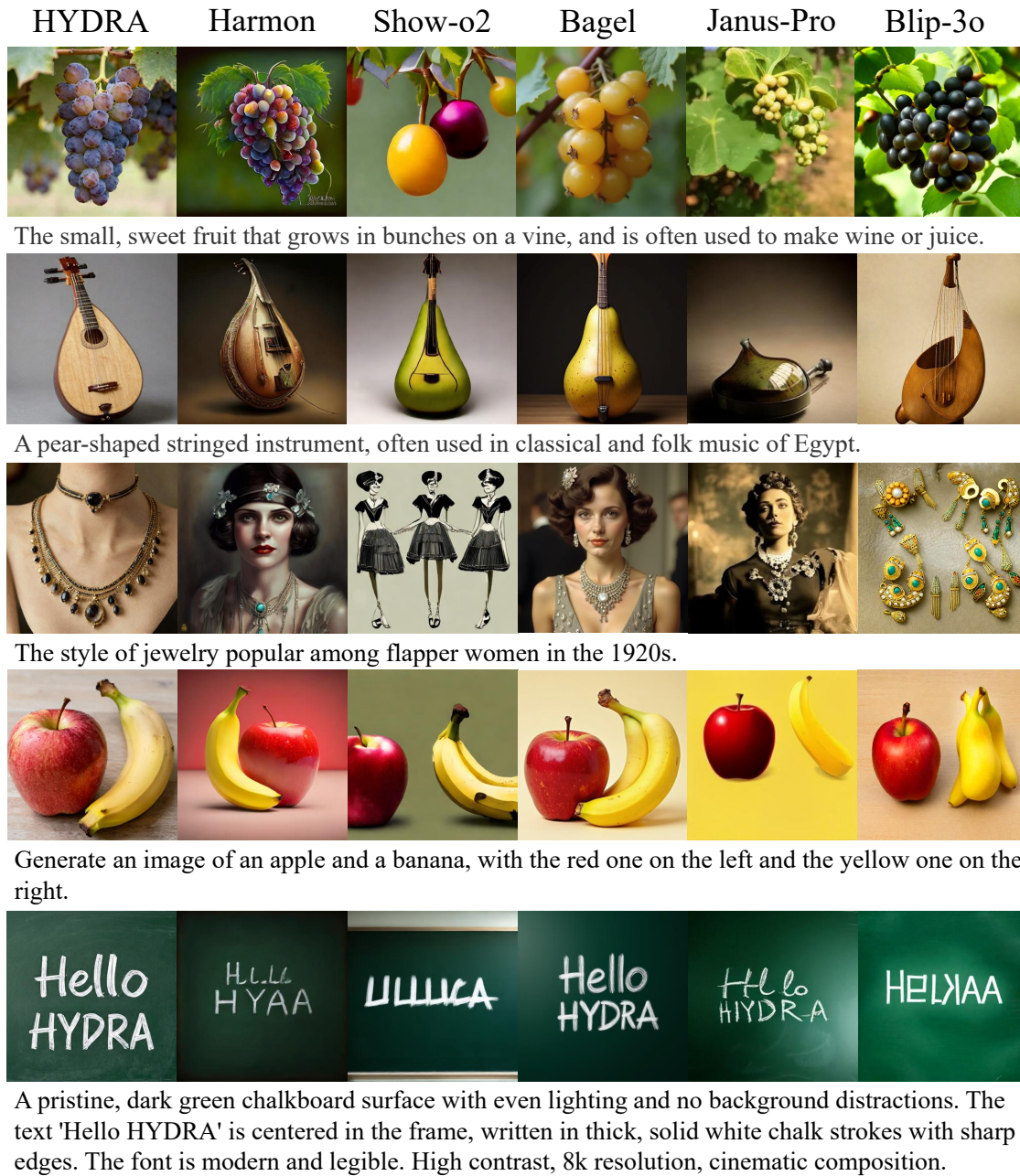


Figure 13. **Qualitative comparison of text-to-image generation.** We compare visual generation results from our HYDRA between Harmon (Wu et al., 2025d), Show-o2 (Xie et al., 2025a), Bagel (Deng et al., 2025a), Janus-pro (Wu et al., 2025b), and Blip-3o (Chen et al., 2025a).

G.3. Multimodal Image Understanding

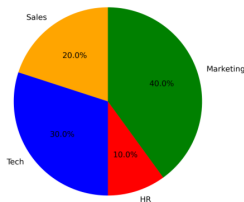
Prompt: Generate the latex code of this formula.

$$A_n = a_0 \left[1 + \frac{3}{4} \sum_{k=1}^n \left(\frac{4}{9} \right)^k \right]$$

Response:

```
\[
A_n = a_0 \left[ 1 + \frac{3}{4} \sum_{k=1}^n \left( \frac{4}{9} \right)^k \right]
\]
```

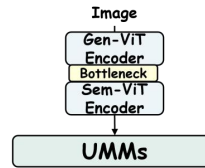
Prompt: Generate the matplotlib.pyplot code for this plot.



Response:

```
import matplotlib.pyplot as plt
labels = ['Sales', 'Tech', 'HR', 'Marketing']
sizes = [20,30,10,40]
colors = ['orange', 'blue', 'red', 'green']
fig, ax = plt.subplots()
ax.pie(sizes, labels=labels, colors=colors,
autopct='%1.1f%%', startangle=90)
ax.axis('equal')
plt.show()
```

Prompt: Describe this image and the algorithm within it.



Response:

The image appears to be a simplified diagram or flowchart representing a conceptual model, possibly related to machine learning or artificial intelligence. It consists of three main components stacked vertically, each labeled with text and accompanied by a smiley face emoji to the left.

At the top is a rectangle labeled "Gen-ViT Encoder," which suggests it could be a genetic variant of a **ViT** encoder, a type of neural network used for image recognition tasks. The term "Gen" might imply a generative aspect or a genetic algorithm component.

Below the "Gen-ViT Encoder" is a smaller rectangle labeled "Bottleneck." This term is often used in machine learning to describe a point in a neural network where the dimensionality of the data is reduced, typically to force the network to learn more abstract features.

The bottom rectangle is labeled "Sem-ViT Encoder," which could indicate a semantic variant of a Vision Transformer encoder. This might be referring to a semantic encoder that processes and interprets the meaning or context of visual data. Beneath these components is a larger rectangle labeled "UMMs," which could stand for "Unified Multimodal Models" or a similar term, suggesting that these encoders are part of a larger framework or system that integrates different models or processes.

Figure 14. **Qualitative results on multimodal image Understanding.** First, HYDRA exhibits superior proficiency in transforming complex visual data into structured text. From accurately generating LaTeX and Python code for formulas and charts to extracting fine-grained details from concept maps, the results highlight its powerful comprehension of diverse and abstract visual inputs.